Master thesis

Fiber coupled sub-nanometer heterodyne displacement interferometry

Delft University of Technology
Faculty of Mechanical, Maritime and Materials Engineering
Department of Precision and Microsystems Engineering
Mechatronic System Design

October 27, 2011

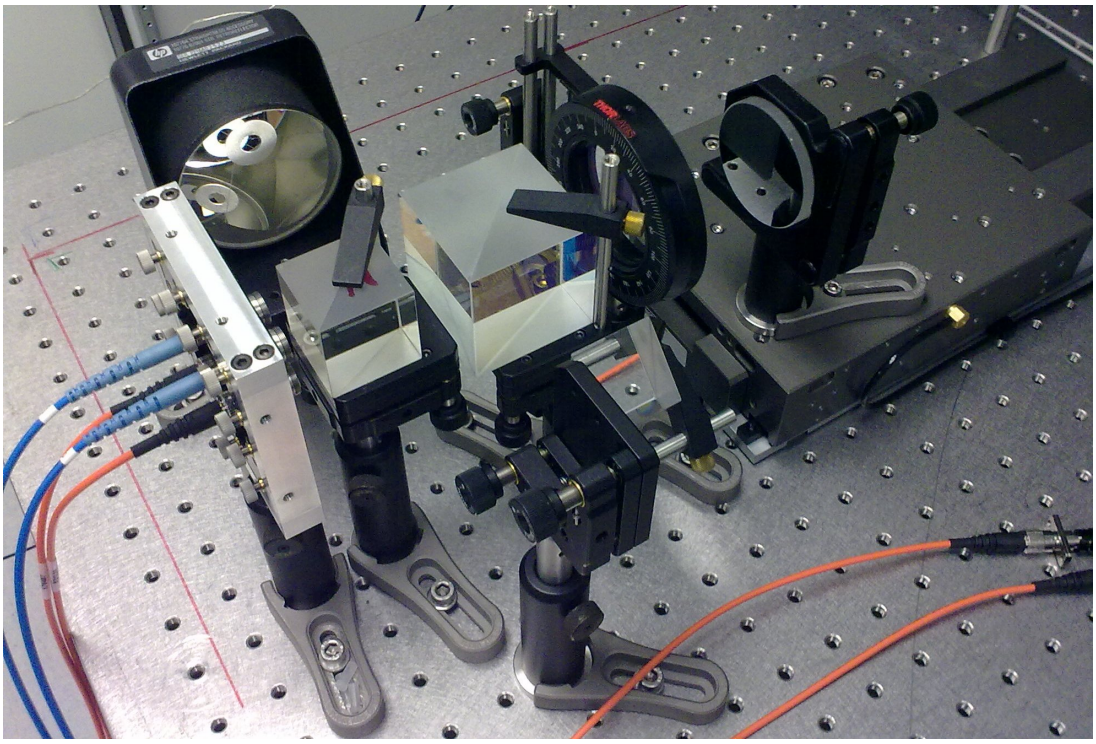

Supervisors:
Prof.ir. R.H. Munnig Schmidt
Ir. J.W. Spronck

Author:
A.J.H. Meskers

Title	Fiber coupled sub-nanometer heterodyne displacement interferometry	
Type of report	Master Thesis	
Report no.	ME 11.030	
Author	A.J.H. Meskers	
Email address	a.j.h.meskers@tudelft.nl	
Student no.	WB1313975	
Examination date	October 27, 2011	
Master specialization	Mechatronic System Design (MSD)	
Department	Precision and Microsystems Engineering (PME)	
Faculty	Mechanical, Maritime and Materials Engineering (3mE)	
University	Delft University of Technology	
Examination board	Prof.ir. R.H. Munnig Schmidt	TU Delft, PME, Mechatronic Systems Design
	Ir. J.W. Spronck	TU Delft, PME, Mechatronic Systems Design
	Dr.ir. P.R. Fraanje	TU Delft, DCSC, Systems and Control
	Dr.ir. W.M. van Spengen	TU Delft, PME, Micro and Nano Engineering

Preface

This report presents the graduation work and its results carried out for the Master Mechatronic System Design at the department of Precision and Microsystems Engineering at the Delft University of Technology. This research was supported by the Dutch Innovative Research Program, IOP (IPT04001).

I would like to thank Jo Spronck for clarification of numerous topics and for his time for discussions, Jonathan Ellis for introducing me to the field of laser interferometry and helping me obtaining my first measurement results and Rob Munnig Schmidt for critically analyzing my work and giving advice.

Furthermore, I would like to thank my friends and family for their support and involvement during obtaining my Master degree.

Arjan Meskers
Delft,
Oktober 2011

Nomenclature and abbreviations

Nomenclature

α	[^{o}]	Angle of exit between modes of an AOM.
κ_1	[-]	Process related factor during lithography, involving feature size.
λ	[m]	Wavelength of applied light.

Abbreviations

AOM	Acousto Optical Modulator.
bs	beam sampler.
BS	neutral Beam Splitter.
CC	Corner Cube reflector.
CD	Critial Dimension.
DOF	Degree Of Freedom.
EUV	Extreme UltraViolet light.
IC	Integrated Circuit.
m	mirror.
Mm	measurement Mirror.
Mr	reference Mirror.
NA	Numerical Aperture.
OI	Optical Isolator.
PBS	Polarizing Beam Splitter.
QWP	Quarter Wave Plate.
RAP	Right Angle Prism.
RR	Retro Reflector.

Keywords

accuracy Relative, mainly qualitative term, indicating the difference between two measurements of which one is more accurate than the other [1].

beat-signal Interference of light results in light varying in irradiance, this could be described by a 'beat'. An interference signal is thus also called a 'beat-signal'.

chip A finished integrated circuit consisting of many semi-conductive layers.

chuck Rigid support for carrying one wafer, equipped with high quality mirrors required for interferometric measurements.

coaxial beam Light beam containing two frequencies with perpendicular linear polarization orientation.

Delft-CC configuration Is the most basic Delft interferometer configuration, using a Corner Cube reflector as target.

Generalized Delft configuration Is more sophisticated than the Delft-CC configuration and used a plane mirror as target.

Delft interferometer Is a type of interferometer which uses spatial separation of optical source frequency pathways throughout the whole interferometer and uses two photodetectors for interference signal detection. Between these detectors a differential measurement takes place.

double patterning This is a process which uses two-step-illumination of the photoresistive layer where during the second illumination a layout is projected onto the photoresist, in between the pattern of the first illumination step.

downtime The period of time when machinery is not in operation as the result of (sub)system malfunction.

exposure system Illumination system without light source.

feature Smallest details in an integrated circuit.

fiber-coupled Transport of light using optical fibers.

free-space Transport of light guided by mirrors through a vacuum or gas.

HeNe-laser Helium Neon laser, referring to the type of gas used for generation of the coherent monochromatic light.

heterodyne-system A system using two light frequencies for operation.

host-system A 'main' system housing sub-systems.

illumination System All system components in between light source and wafer, located inside a lithography machine.

iris An iris is an adjustable diaphragm allowing for variation of an optical free pathway diameter.

interferometer group of optical components responsible for light interference measuring one DOF.

laser source A laser which generates monochromatic coherent light.

lithography A printing process where the image to be printed is projected on a flat surface consisting of photoresist, and is treated to construct physical geometries.

lithography machine A machine with the sole purpose of projection of the layout of a reticle onto photoresistive material.

mm-fiber Graded index Multi Mode fiber.

non-ideal laser source A laser source generating a heterodyne coaxial beam allows for polarization thus frequency mixing, resulting in the presence of periodic nonlinear errors.

optical recombination box Complex optical sub-system inside a lithography machine consisting of multiple optical components for recombination of two source light beams into a coaxial beam.

overlay error Positional mismatch between two adjacent layers during IC manufacture.

patterning A term referring to the projection of a layout from the reticle onto photoresistive material.

periodic error Periodic nonlinear errors are caused by polarization and frequency mixing, it prevents measuring with sub-nanometer uncertainty.

photoresistive material Also called 'photoresist', the properties of this light sensitive material alter when exposed to light.

pm-fiber Polarization Maintaining single mode fiber.

resolution The smallest change in a quantity being measured that causes a perceptible change in the corresponding indication [1].

reticle stage The stage carrying the layout for one layer of an IC.

robustness Guaranteeing stability and performance requirements during and after parameter variations.

source frequency Stable and pure base frequency delivered to an interferometer, used for measurements.

sub-nm Sub-nanometer.

target A target for an interferometer normally consists of a chuck or reticle stage; for research purposes the target for this report consists of either a corner cube reflector or a plane mirror on top of a one DOF air bearing stage.

uncertainty A non-negative parameter, characterizing the dispersion of the quantity values, being attributed to a measurand, based on the information used, including all random and non-compensated systematic errors [1].

wafer Silicon substrate carrying integrated circuits during manufacture.

waferstage Location where wafers are prepared for-, pattering.

yield The ratio between functional and non-functional units.

[1] R. M. Schmidt, G. Schitter, and J. van Eijk, *The Design of High Performance Mechatronics*. IOS Press under the imprint Delft University Press ISBN 978-1-60750-825-0, 2011.

Summary

The integrated circuit industry builds integrated circuits (IC's) by placing many layers of semi-conductive material on top of each other, the smallest details in such a layer are called *features*. Each layer has its own specific layout and will form together with the other layers three dimensional structures such as transistors, diodes or resistors. The final result is an integrated circuit which is called a *chip* of which a large number of them are fabricated all at once on a round silicon *wafer*. A position error between these two layers is called an *overlay error*, the final chip might not function correctly or not at all if this overlay error exceeds certain limits. It is important to minimize this error to obtain a high yield per wafer.

As the features are getting smaller in size, the position of a 'new' layer with respect to the layer below becomes more critical. High end position measurement equipment is required to minimize this overlay error. The *lithography-machines* involved with the production of these IC's are expensive due their advanced technology and are therefore subject to high wafer throughput to reduce costs. These processes require thus a measurement tool which can measure with low measurement uncertainty to minimize the overlay error, while allowing for high target velocity. A laser interferometer is such a measurement tool which is able to measure accurate and fast enough to be used for these processes.

The laser light required by interferometers to operate in current lithography-machines is guided along corners by mirrors, over meters long optical pathways. This method of light transport is sensitive for environmental disturbances and requires realignment once maintenance is carried out, this is a time consuming and thus costly process. The current interferometer systems also contain small *periodic nonlinearities*, this nonlinear error presence in the position measurements will become problematic for future systems which require increasingly smaller overlay errors.

At the TU Delft a theoretical periodic error free type of interferometer has been build (see Figure 6), based upon spatial separation of optical measurement pathways. This system has shown to operate with sub-nm measurement uncertainty (see *Appendices B.1* and *B.2*) using *free-space* source frequency delivery. Replacing the free-space beam delivery by *fiber-coupled* delivery allows for modular plug-and-play systems. No more sensitive to air turbulence, but the light transported by the fibers is unfortunately negatively affected by several phenomena and requires more in depth research.

The *Delft interferometer* concept (Figure 6) knows multiple configurations, two of them have been build for this research: the *Delft Corner Cube*- and the *Generalized Delft*-configuration. Three measurement systems have been realized to research operation when the source frequencies are delivered by different types of fibers. The first system, *System I*, concerns the *Generalized Delft configuration* with free-space beam delivery with the purpose of reproduction of previous results (see *Appendices B.1* and *B.2*). The obtained results serve as reference for the measurements obtained from the second system, *System II*. In this system the source frequencies are delivered by polarization maintaining single mode fibers (i.e. *pm-fibers*) instead of mirrors. The second system was build study the sub-nm measurement uncertainty using these pm-fibers for beam delivery, instead of free-space beam delivery. The results obtained from this research are published in the first article of this report, *Article I: Fiber-coupled displacement interferometry without periodic nonlinearity*.

The third measurement system, *System III*, was build to research the performance of graded index multi mode fibers (i.e. *mm-fibers*) for source frequency delivery for the *Delft Corner Cube* configuration. These fibers allow for easier alignment and higher optical coupling efficiency compared to pm-fibers. However the ease in handling results in lower optical output quality: the fiber does not maintain polarization state, the initial optical wavefront will be deformed during transport and multiple optical modes will be present

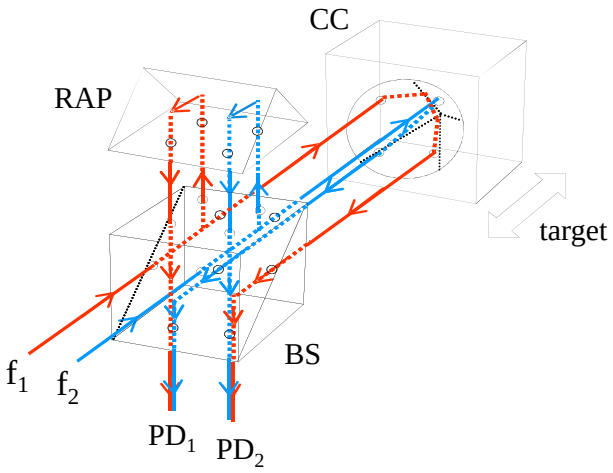

Figure 1: *The interferometer depicted in the image has two spatially separated source frequencies f_1 and f_2 coming in at the left. The optical pathways of these two beams are kept separated throughout the whole interferometer. This 'Delft' interferometer configuration is called the 'Delft Corner Cube' interferometer configuration.*

in its output. The results obtained with this system are published in the second chapter of this report, *Article II: Displacement interferometry with fiber-coupled delivery*.

Conclusions from the research:

Yes, it is possible to measure with sub-nm measurement uncertainty using pm-fiber delivered source frequencies for the *Generalized Delft interferometer*. We have shown that the periodic nonlinearity was not visible down to the noisefloor ($\sim$40pm). The same conclusion holds for mm-fiber delivered source frequencies using the *Delft Corner Cube interferometer*.

Both fiber-coupled systems show phase broadening behavior in their measurement results, caused by the birefringent nature of the fibers. This behavior can be seen best in the results using mm-fibers. At first sight this fortunately does not affect the measurement uncertainty.

Experimental results confirm that fiber induced phase shifts caused by fiber deformation, are canceled out due the configuration of the *Delft interferometer* and the differential measurement between the photodetectors.

The time varying polarization orientation of the light delivered by mm-fibers in *System III*, results in interference fluctuations as expected. Nevertheless, the interference signal was not lost during measurements and the fiber coupled system can still measure with sub-nm measurement uncertainty.

Building the two fiber coupled systems (*System II & III*) has shown that pm-fibers require much effort regarding alignment and obtaining a sufficiently high optical coupling efficiency. The finally achieved optical output was of high quality. Multi mode fibers behaved opposite, they were very easy in handling but resulted in a less high optical output quality.

Using fiber delivery for the *Delft interferometers* opens the way towards the design of a modular fiber-coupled sub-nm interferometer measurement system. The optical symmetry of the design has shown to be very robust towards phase disturbances, but more research is required regarding system robustness and applicability.

Contents

Introduction

In many products such as mobile phones, camera's, refrigerators, etc. you can nowadays find microchips which are responsible for the control inside a product. Miniaturization of these chips and other electro-/mechanical components cause these products to operate faster, smarter and more energy efficient which is primarily required for the smaller high tech hand held devices. This decrease in component size makes the semiconductor industry (manufacturing integrated circuits i.e. IC's) one of the most demanding industries when it comes to detail size and positioning accuracy during their manufacturing processes. Sizes and accuracies in the order of a nanometer and less have become standard.

Manufacturing IC's consists of placing many interconnected layers of semi-conductive material on top of each other. Each new layer has its own specific layout and will form together with the other layers three dimensional structures such as transistors, diodes or resistors. The final result is an integrated circuit which is called a *chip* of which a large number of them are fabricated all at once on a round silicon *wafer*[1]. Each new layer is 'printed' on top of its layer below during a process called *lithography*. Creation of one layer requires a number of process steps: I) deposition of *photoresist*, II) illumination of photoresist and III) etching (multiple times), shown in Figure 2. These steps are repeated for each layer until the chip is finished. In reality these steps and processes can become quite complex depending on the wanted chip architecture.

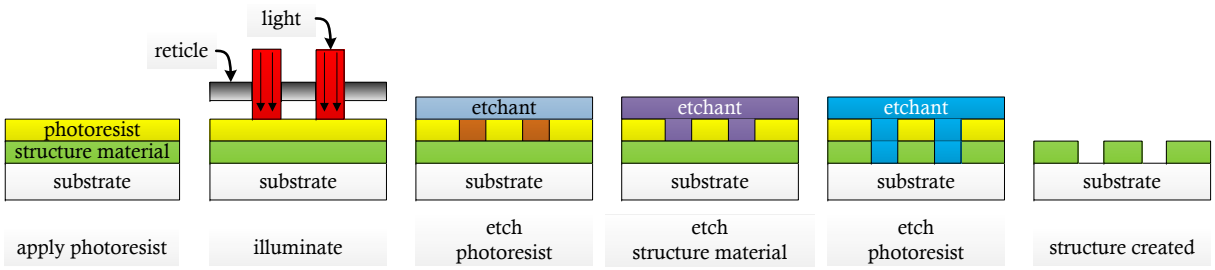

Fig. 2: *The schematic representation above shows a few steps of a lithography process for creating one structural layer of an IC. The first step consists of deposition of photoresistive material (left). The second step is illumination of this photoresist using a patterned mask (also called a* reticle*), the layout for the new layer is projected onto the photoresist. This causes certain areas to be illuminated and some areas not. The material properties of the photoresist change due to illumination and the next step, 'etching' will either remove the illuminated material or the non-illuminated material. The etching steps are repeated until the resulting layer is obtained.*

The layout of a layer is determined during the illumination process (see Figure 2 'illuminate' step) where the reticle layout is transferred onto the photoresistive material. The size of the smallest details (the features) that can be projected onto the photoresist are primarily limited by the optical resolution of the exposure system. The resolution of this system is indicated by its Critical Dimension (CD), Equation 1, which determines the maximum obtainable resolution as a function of several parameters such as: the wavelength in vacuum of the light used for illumination λ, the Numerical Aperture (NA) of the lens(es) and a so called 'κ_1'-factor which is determined by the illumination system.

$$CD = \kappa_1 \frac{\lambda}{NA} \tag{1}$$

[1]Current wafer diameters are around 300mm, the next generation machines are expected to use 450mm diameter wafers. This increase in size which will impose numerous new 'challenges' in the development of the manufacturing equipment.

The next generation lithography machines will use an Extreme UltraViolet (*EUV*) light source to decrease the feature size by using light with a decreased wavelength, λ. As the features are getting smaller in size, the position of a 'new' layer with respect to the layer below becomes more critical. A position error between these two layers is called an *overlay error*. The final chip might not function correctly or not at all if this overlay error exceeds certain limits, it must therefore be minimized in order to obtain a high yield per wafer.

The periodic enhancement in the resolution achieved through photolithography has been a driving force behind Moore's Law. Resolution improvements enable printing of smaller features for an integrated circuit, Figure 3 shows the decrease of feature size over the years. In the year 2011 the aimed feature size is 22nm, allowing for a maximum overlay-error of not more than 6.6nm[2] (i.e. 30%). Machines which utilize a so called *double patterning process* require even smaller overlay errors for their processes, 15% at maximum.

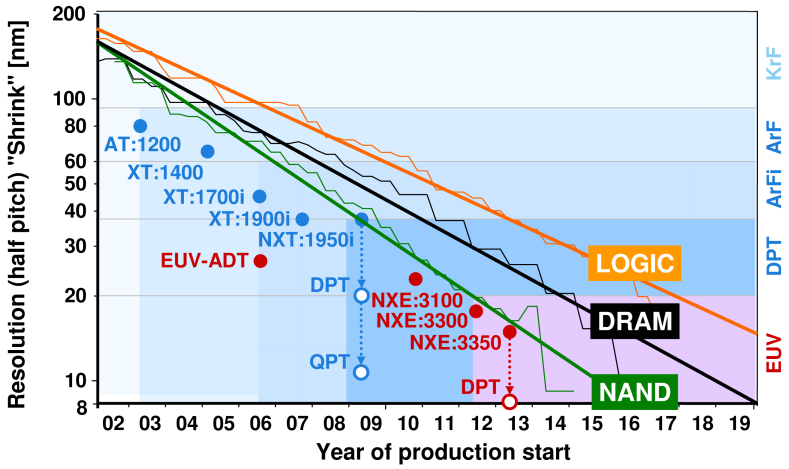

Fig. 3: *Each subsequent year (horizontal axis) the feature size (left vertical axis) decreases. The applied fabrication techniques are mentioned at the right vertical axis. The abbreviation 'DPT' stands for double patterning which is a solution for decreasing the feature size using a two step patterning process. The EUV machines (Extreme UltraViolet) are single process machines which use EUV-light for illumination, they are able to pattern details down to 13nm due to the short wavelength used.*
The terms 'Logic', 'NAND' and 'DRAM' refer to the types of circuits which are generally fabricated. Each type has its own requirements. The 'NAND'-type of structure for example can be found in USB-sticks while 'DRAM' is used as working memory in PC's.

High end position measurement equipment is required to minimize the overlay error by measuring with low measurement uncertainty while allowing for high wafer throughput (referring to targets moving at high accelerations and velocities). A laser interferometer is such a measurement tool which is able to measure accurate and fast enough. A lithography-machine using interferometers for these reasons is an ASML 'Twinscan' machine, shown in Figure 4(a). Inside this machine (i.e. *host-system*) there are two locations where interferometers are applied. The first location is the reticle stage where the layout of each layer originates from and the second location is the so called *waferstage* where the wafers are handled. The position of each wafer is continuously measured by interferometers by measuring the position of the *chucks* that carry the wafers. The wafer at the far most right is scanned for its topology as preparation for the patterning process, shown at the left.

The light required for the interferometers is generated by a laser source located outside the host-system to reduce internal thermal effects. In current systems the light generated by the laser source is a heterodyne coaxial light beam containing two frequencies with a perpendicular oriented linear polarization state, see Figure 5. This light is split into two beams each containing one frequency and is transported towards the host-system by means of two optical fibers. The other ends of the fibers are connected to a so called *optical recombination box* which is located at the interface with the host-system. This box recombines the two frequencies again into a coaxial heterodyne beam, that is split multiple times to foresee multiple interferometers with these source frequencies. The transport of the beams inside the host-system currently

[2]For dimensional insight, 1nm is 4 silicon atoms across.

(a) (b)

Fig. 4: *The ASML 'Twinscan' machine shown in figure 4(a) is used in the manufacturing process of IC's and is an example of a system where interferometers for displacement measurement are used. In image 4(b) a more detailed overview of the waferstage is given, the red lines depict laser light used by the interferometers for measuring displacement. At the top is the reticle stage located while at the bottom two wafers are handled. The laser interferometers continuously measure the multiple degrees of freedom of the two chucks and the reticle stage. (www.asml.com)*

consists of mirrors guiding the light along corners, over meters long optical pathways. These mirrors all have to be realigned once maintenance is carried out, this is a time consuming and thus costly process.

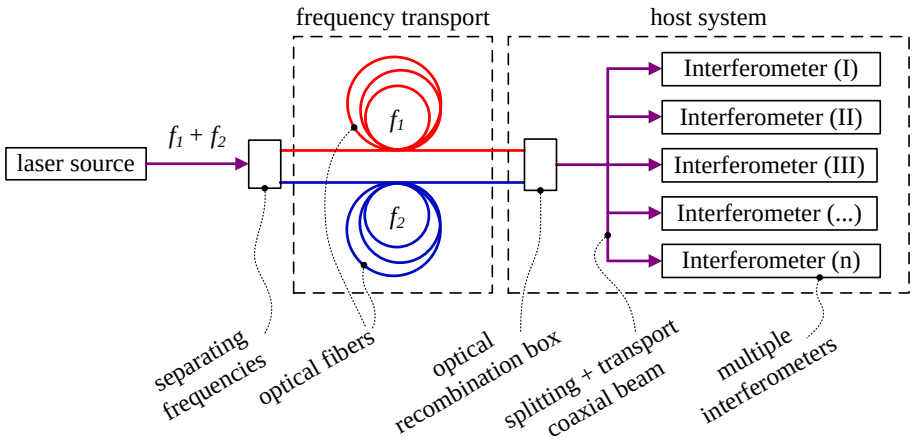

Fig. 5: *A laser source generates a coaxial beam carrying f_1 and f_2 which are split and launched into two separate fibers. These fibers transport the source frequencies towards the host system where they are connected to a so called 'optical recombination box' which is a complex optical system recombining the fiber outputs again into one coaxial beam. The light exiting this box is then guided over meters by means of mirrors and beamsplitters towards a multitude of interferometers.*

The system depicted in Figure 5 operates well and is able to measure relative target displacements at high resolution with sub-nanometer (sub-nm) uncertainty. But the system also contains small *periodic nonlinearities* leading to increased measurement uncertainty. The presence of this error in the position measurements becomes problematic for future systems which require increasingly smaller overlay errors.

The Delft University of Technology (TU Delft) has build a theoretical periodic error free type of interferometer (see Figure 6), based upon spatial separation of the two source frequencies throughout the whole system, until just before the light reaches the photodetectors. This design prevents the periodic error by separation of optical pathways, eliminating polarization- and frequency mixing causing this type of error. This system has shown to operate with sub-nm measurement uncertainty (see *Appendices B.1* and *B.2*)

using *free-space* source frequency delivery, but it is sensitive (low robustness) to disturbances. Replacing free-space beam delivery by *fiber-coupled* delivery allows for less sensitive (increased robustness) plug-and-play systems. The light transported by optical fibers is unfortunately negatively affected by several phenomena and requires therefore investigation.

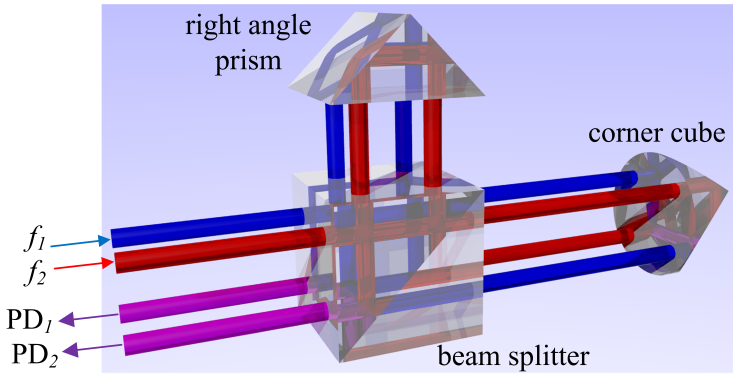

Fig. 6: *The image shows the most basic configuration of the Delft interferometer. Two source beams f_1 and f_2 entering at the left, are split 50/50 at the beamsplitter. The light for creating a reference is reflected upwards into a right angle prism and transfers the light to the photodetectors (PD_1 and PD_2) via the beamsplitter. The other 50% of the split light is reflected by the corner cube and translated diagonally after which it reaches the two photodetectors by passing the beamsplitter for a second time. The corner cube reflector is attached to the target of which the (relative) displacement is to be measured.*

Project description and objective

The *Delft interferometer* concept (Figure 6) knows multiple configurations, two of them will be build for the research. They are the *Delft Corner Cube-* and the *Generalized Delft-*configurations. With the use of these two interferometers, three measurement systems have will be constructed. The purpose of these systems is to investigate operation when the source frequencies are delivered by different types of fibers. The first system, *System I*, concerns the *Generalized Delft configuration* with free-space beam delivery with the purpose of reproduction of previous results (see *Appendices B.1* and *B.2*). The obtained results will serve as reference for the measurements obtained from the second system, *System II*. In this system the interferometer configuration stays unaltered but the source frequencies are delivered by polarization maintaining single mode fibers (i.e. *pm-fibers*) instead of mirrors. The resulting differences between the first and the second system are the result of the utilization of the fibers. The purpose of this second system is to investigate whether is possible to measure with sub-nm uncertainty using these pm-fibers for beam delivery, instead of free-space beam delivery.

The third measurement system, *System III*, has as purpose to investigate the performance of graded index multi mode fibers (i.e. *mm-fibers*) for source frequency delivery for the *Delft Corner Cube* configuration. These fibers allow for easier alignment and higher optical coupling efficiency compared to pm-fibers. Unfortunately the ease in handling will result in lower optical output quality: the fiber does not maintain polarization state, the initial optical wavefront will be deformed during transport and multiple optical modes will be present in its output.

The objective of above described research is to investigate the performance of the two Delft interferometer configurations when using fiber delivered source frequencies.

Article I:
Fiber-coupled displacement interferometry without periodic nonlinearity

This article is published in the scientific journal: *Optics Letters*, on September the 15^{th} of 2011 and contains results that were also presented at the 10th International Symposium of Measurement Technology and Intelligent Instruments (ISMTII) from June 29 till July 2nd, 2011 in South Korea (included in *Appendix B.3*).

The purpose of this research was to investigate the performance of the *Generalized Delft interferometer* configuration (see *Appendix A.4*) when using polarization maintaining single mode fibers (*Appendix A.3*).

Article II:
Displacement interferometry with fiber-coupled delivery

The results described in this article are presented at the 10th IMEKO Symposium for Laser Metrology for Precision Measurement and Inspection in Industry, from September 12 till 14, 2011 in Germany.

The research performed is a continuation of previous research described in *Article I* and *Appendix B.3*. In this second article also fiber coupled delivery is applied, but now using a different type of fiber and a different *Delft interferometer* configuration (see also *Appendix A.4*).

The purpose of this research was to investigate the performance of the *Delft Corner Cube interferometer* configuration (see *Appendix A.4*) when using graded index multi mode fibers (*Appendix A.3*).

Displacement interferometry with fiber-coupled delivery

Arjan J.H. Meskers[1], Jonathan D. Ellis[2], Jo W. Spronck[1*], and Robert H. Munnig Schmidt[1].

1 PME: Mechatronic System Design, Delft University of Technology, Mekelweg 2, 2628 CD Delft, The Netherlands.

2 Mechanical Engineering Department & Institute of Optics, University of Rochester, Hopeman Building, Rochester NY, 14627, USA

* Corresponding Author / E-mail: j.w.spronck@tudelft.nl, TEL: +31-15-278-1824

Abstract:

Heterodyne interferometry is a widely applied technique for length and displacement measurements in precision systems. Free-space optical beam delivery couples the source directly to the interferometer location. Conversely, fiber delivery is desired to decouple the source and interferometer. Drawbacks to using fibers are either time consuming alignment (PM fiber) or time varying polarization output (MM fiber). Jones matrices were used to analyze Joo-type interferometers to simulate the effects of using MM fiber inputs. The results showed loss of interference at some instances from the rotating polarization states. Measurements with a MM fiber coupled interferometer showed minimal polarization rotation and no interference loss.

Introduction and Motivation

Heterodyne displacement measuring interferometry is a widely applied technique which uses two beams at slightly different optical frequencies to measure displacements by measuring the optical path length change between reference and measurement arms. It is known for its high dynamic range, high signal-to-noise ratio, and direct traceability to length standards [1]. Primary applications for such a system can be found in calibration of other measurement tools such as capacitive sensors, inductive sensors, and optical encoders. Sub-nanometer level measurements must be achieved to satisfy industrial demands on performance [2]. The main error sources that limit the performance are the laser frequency stability [1], refractive index fluctuations in non-common optical paths [3], and periodic nonlinearity [4-5] in the measured phase due to frequency mixing, polarization mixing and a combination of polarization-frequency mixing [6]. Causes of mixing can be found in non-ideal optical

alignment and manufacturing tolerances (i.e. leakage, ghosting).

Previously, we demonstrated three different Joo-type interferometer configurations which had no detectable periodic nonlinearity when employing free-space delivery [7-9]. Recently, we have also reported the Generalized Joo-type interferometer can be fiber delivered with two polarization maintaining fibers (PM fibers) while eliminating the fiber-induced Doppler shifts and maintaining a periodic error free measurement [9].

The Joo-type interferometer is characterized by two spatially separated source beams with a known frequency offset, which are held separate until a final interference surface. Periodic nonlinearity is significantly reduced by postponing beam overlap until the final interference surface [10-13].

When applying fiber delivery, a number of potential error sources are introduced. Fiber induced Doppler shifts due to stretch of the fiber can be mitigated by generating an optical reference after the fibers, one of the advantages of this design. Stress induced birefringence will however distort the source beam's original wave front and polarization state. Most fiber delivered systems will show a decrease in polarization state [14]. For a system where optical fibers are employed, this is often the largest source for polarization degradation. Polarization clean-up can be applied after fiber outcoupling [15, 16] using a polarizer, but this reduces the available optical power. Employing PM fibers reduces this effect but also increases the complexity and required robustness of the optical coupling between fiber and source.

In this proceeding, we discuss the possibilities and limitations with using MM fibers instead of PM fibers for Joo-type interferometer fiber delivery. We employ a Jones Matrix model of the Joo Retroreflector Interferometer including the time varying polarization effects in MM fibers.

The Joo Retroreflector Interferometer

The fiber-coupled Joo Retroreflector Interferometer, Figure 1, is the simplest form of the Joo-type interferometer configurations with fiber input coupling. Two optical beams with slightly different frequencies are delivered via two fibers. After delivery, a beamsplitter (BS) is used to split the spatially separated incoming beams into measurement and reference arms. The reference arms reflect via a vertical right angle prism (RAP) while the measurement arms reflect off a retroreflector (RR) attached to the target. The irradiance signals detected by PD_1 and PD_2 are of the form

$$I_1 \propto \cos\left(2\pi f_s t + \theta_1 - \theta_2 - \theta_r\right) \text{ and} \qquad (1)$$

$$I_2 \propto \cos\left(2\pi f_s t + \theta_1 - \theta_2 + \theta_r\right) \quad (2)$$

where f_s is the heterodyne split frequency, θ_1 is the fiber Doppler shift of beam *1*, θ_2 is the fiber Doppler shift of beam 2, and θ_r is the phase change due to retroreflector motions. The measured phase change, θ_r, is the difference between the phases of I_1 and I_2 or $\left|\left(\theta_1 - \theta_2 - \theta_r\right) - \left(\theta_1 - \theta_2 + \theta_r\right)\right| = 2\theta_r$, where the fiber Doppler shifts cancel. The measured phase is related to the retroreflector displacement by $\theta_r = \frac{2\pi N n z}{\lambda}$, where N is the interferometer fold constant (N = 4), n is the refractive index, z is the optical path length difference, and λ is the optical wavelength.

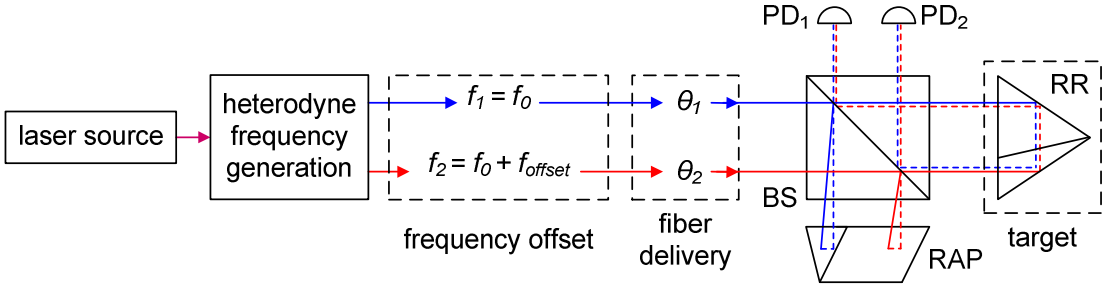

Figure 1: Schematic the fiber coupled Joo Retroreflector Interferometer. Generation of the heterodyne source beams, with a frequency offset between them at the left, fiber-coupled delivery in the middle and the Joo Retroreflector Interferometer at the right.

Previous research

One of the concerns with the fiber delivery is limiting the polarization leakage of the unwanted polarization state into the system. Because a PM fiber has two different stress states (anisotropic core) and no coupling is ever perfect, some light will pass through the unwanted polarization state. Stress in the fiber should largely be common mode between the two polarizations states but the different stress levels can result in a minor difference, potentially leading to periodic nonlinearity.

In practice, this effect can be minimized with proper alignment techniques. The fiber delivery induced Doppler shifts do cause attenuation in vibration peaks in the Fourier domain. Figure 2 shows the error amplitude in the fringe domain for forwards and backwards traces for both fiber-delivered and free-space delivered Generalized Joo Interferometer [9], with a stage traveling at ±100 μm/s. The shifts between forwards and backwards motions are attributed to stage induced vibrations which change based on the Doppler direction. In the free-space

measurements, the peaks at 0.8 and 1.2 Fringe Orders are sharp compared to their respective fiber delivered measurements.

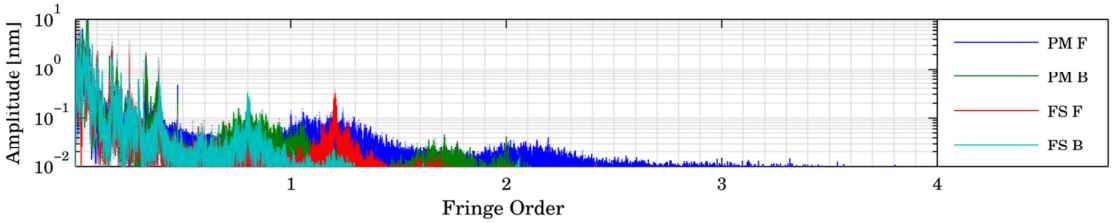

Figure 2: Error amplitude for 100 µm/s linear forwards and backwards traces using the Generalized Joo Interferometer [9]. The fiber-coupled setup shows broadening of Fringe Orders, possible due to fiber dispersion [17]. (PM: polarization maintaining, FS: free-space, F: forwards trace, B: backwards trace).

Multimode Fibers and Polarization Rotation

Employing polarization maintaining fibers requires tight tolerances on the input beam alignment, both in space and polarization. Conversely multimode fibers can be used with only minor tolerances but will cause a random polarization state to be launched from the fiber into the system. The equivalence of a multimode fiber can be simulated by a uniform element possessing both linear and circular birefringence (i.e. a retarder/rotator pair [17]) built using Jones matrices [18]. With a horizontal fast axis for the retarder as

$$J_{mm}(\theta_i) = \prod_{i=1}^{M} P_i \cdot R_i = \begin{bmatrix} e^{j\Delta\tau_i/2} & 0 \\ 0 & e^{-j\Delta\tau_i/2} \end{bmatrix} \begin{bmatrix} \cos(\theta_i) & \sin(\theta_i) \\ -\sin(\theta_i) & \cos(\theta_i) \end{bmatrix} \tag{3}$$

where i is the fiber segment, M is the number of fiber segments (usually >100), P_i is the relative polarization delay matrix, R_i is rotation matrix, j is $\sqrt{-1}$, τ_i is the time delay, θ_i is the instantaneous angle of rotation, and φ_i is the instantaneous phase of the incoming wave. Because the fibers in this research are short (<10 m), the relative polarization delay between orthogonal polarization states is negligible [18]. However, the outcoming polarization can be anywhere between 0 and 2π. This presents a problem because two fibers are used to launch light into the interferometer, which means there will always be a situation where the outcoming polarizations states can be orthogonal, eliminating interference. The complete MM, fiber-coupled Joo retroreflector interferometer can be using Jones matrices since little depolarization occurs (where Mueller matrices would be better suited). The modeled irradiance at the detector is

$$I = \Re\left[\left(J_{bs}J_{rap}J_{bs}J_{mm,1}E_1\right)\bullet\left(J_{bs}J_{rr}J_{bs}J_{mm,2}E_2\right)\right] \quad (4)$$

where I is modeled irradiance; J_{bs}, J_{rap}, and J_{rr} are the Jones matrices for the beamsplitter, right angle prism, and retroreflector, respectively; $J_{mm,1}$ and $J_{mm,2}$ are the MM fiber matrices, and E_1 and E_2 are the two input electric field vectors. In this case, we only model one irradiance value at the detector because the polarization states are the same at both detectors. If the output rotations of $J_{mm,1}$ and $J_{mm,2}$ are varied at different rates, the normalized irradiance at the detector has specific instances where it loses the heterodyne signal, Figure 3. One potential solution to the interference loss problem is to use multimode-polarization maintaing fiber which has a larger core for easier coupling but maintains some fixed polarization output [19].

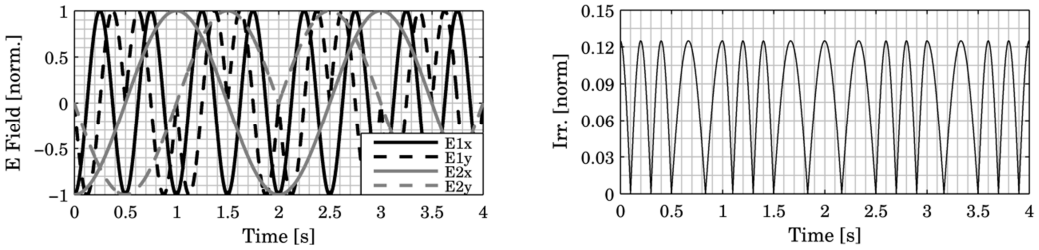

Figure 3: (left) Simulated electric field amplitude changes for the assessing the fiber output polarization. (right) Detected irradiance as the input fibers continuously change orientation, causing signal loss when the signals are orthogonal.

Multimode and Polarization Maintaining Fiber Measurements

A general Joo Interferometer has been tested using both MM and PM fibers, Figure 4. Since the polarization state from MM fibers did not lose interference, sufficient signal was obtained to measure similar stage motions as with the PM fiber configuration. However, further experiments are needed to characterize the MM fiber effects for this purpose.

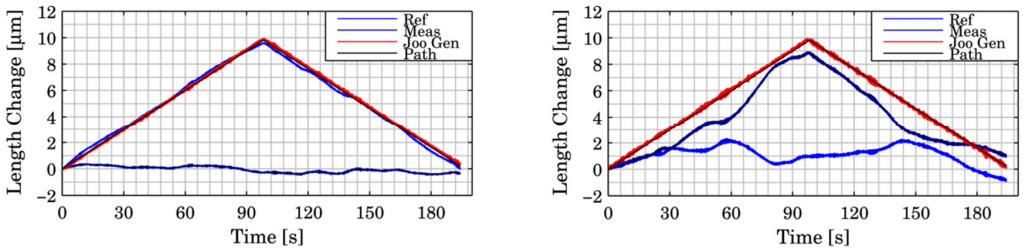

Figure 4: Forward and backward scans of an air bearing stage measured with a Generalized Joo Interferometer using MM fibers (left) and PM fibers (right). The fluctuations of the measurements in blue are from fiber induced Doppler shifts.

Conclusions

The effect of a time varying polarization state analysis for a fiber coupled Joo Retroreflector Interferometer using Jones matrices has been described. The analysis shows when heterodyne source beams are assumed to be linearly polarized and rotate independently over time, there will be an instance that the interference signal is lost due to perpendicular polarization states. Measurements in which multimode fibers were employed showed no loss of signal during minor fiber disturbances. During fiber transport, the ideal linear polarization states will be altered, which is more present in MM fibers than in PM fibers. Further research is needed on the relationship between output polarizations in MM fibers relative to the applied stress on the fibers.

This work was performed at the Delft University of Technology and supported by the Dutch IOP (IPT04001) in the Netherlands.

REFERENCES

[1] Bobroff N, *Meas. Sci. & Technol.*, 1993, **4**(9): 907-926

[2] Demarest FC, *Meas. Sci. Technol.*, 1998 **9**(7): 1024-1030

[3] Estler WT, *App. Opt.*, 1985 **24**(6): 808-815

[4] Quenelle RC, *Hewlett Packard J.*, 1983 **34**: 10

[5] Hou W and Wilkening G, *Precis. Eng.*, 1992 **14**(2): 91-98

[6] De Freitas JM and Player MA, *J. Mod. Opt.*, 1995 **42**(9): 1875-1899

[7] Joo K, *et al., Opt. Lett.*, 2009 **34**(3): 386-388

[8] Joo K, *et al., Opt. Exp.*, 2010 **18**(2): 1159-1165

[9] Meskers AJH, *et al.*, *Proc. 10th ISMTII,* 29Jun-2July, Daejeon, South Korea, 2011.

[10] Tanaka M, *et al.*, *IEEE Trans. Instrum. Meas.*, 1989 **38**(2): 552-554

[11] Wu C, *et al.*, *App. Opt.*, 1999 **38**(19): 4089-4094

[12] Lawall J and Kessler E, *Rev. Sci. Instrum.*, 2000 **71**(7): 2669-2676

[13] Schuldt T, *et al., Class. Quan. Grav.*, 2009 **26**(8): 085008

[14] Simon R, *Opt. Comm.*, 1990 **77**(5-6): 349-354

[15] Knarren BAWH Technical University of Eindhoven: PhD Thesis, Netherlands, 2003.

[16] Knarren BAWH, *et al., Precis. Eng.*, 2005 **2**: 229-236

[17] Rogers A, *Understanding Optical Fiber Communications,* Artech House, 2001

[18] Sundsoy PR, Norwegian University of Science and Technology: MSc Thesis, Norway, 2004

[19] Furukawa RA, *et al.*, Appl. Phys. Lett., 2008 **93**(10): 103303

Conclusions

The *Generalized Delft-* and the *Delft Corner Cube* configurations are both able to measure with sub-nm measurement uncertainty when the source frequencies are delivered by pm-fibers (*System II*) and mm-fibers (*System III*). We have shown that the periodic nonlinearity was not visible down to the noisefloor ($\sim$40pm). These are positive results since they give the opportunity for development towards a modular fiber-coupled interferometer measurement system, measuring with sub-nm uncertainty.

Both fiber-coupled systems show phase broadening behavior in their measurement results, caused by the birefringent nature of the fibers. This behavior can be seen best in the results using mm-fibers. At first sight this fortunately does not affect the measurement uncertainty.

Experimental results confirm that fiber induced phase shifts caused by fiber deformation, are canceled out due the configuration of the *Delft interferometer* and the differential measurement between the photodetectors.

The time varying polarization orientation of the light delivered by mm-fibers in *System III*, results in interference fluctuations as expected. Nevertheless, the interference signal was not lost during measurements and the fiber coupled system can still measure with sub-nm measurement uncertainty.

Building the two fiber coupled systems (*System II & III*) has shown that pm-fibers require much effort regarding alignment and obtaining a sufficiently high optical coupling efficiency. The finally achieved optical output was of high quality. Multi mode fibers behaved opposite, they were very easy in handling but resulted in a less high optical output quality.

The optical symmetry of the design has shown to be very robust towards phase disturbances, but more research is required regarding system robustness and applicability. This is done by performing further research using different *Delft Interferometer* configurations and fiber types, as part of a Ph.D research. System characterization can be done by carrying out the following tests:

1. Comparison of measurement-data of the *Delft interferometer* for different beam delivery methods (free-space and different fiber types).
2. Research the different fiber disturbance effects and their impact on measurement output, such as:
   - Polarization orientation, -stability- and quality.
   - Phase broadening, -shift and quality.
3. Investigate the efficiency and stability of the fiber couplings, related to measurement output quality.
4. Study the requirements for operating in vacuum environments and research the *Delft interferometer* performance in such an environment.
5. Investigate the idea that coiling mm-fibers might increase output quality or reduce negative transport effects for mm-fibers.
6. Study techniques to measure and optimize wave front deformation.

Investigation of fiber behavior in combination with a certain *Delft interferometer* configuration is important, but the operation of this type of interferometer itself also allows for much more in depth research. Some topics regarding the interferometer itself which can be further investigated, are:

1. The periodic error free operation of the *Delft-interferometer* design.
2. If the alignment robustness will increase when the right angle prism is replaced by two corner cubes.
3. Beam-walk-off behavior (change location of phase) for angular measurements.
4. The performance of a specific *Delft interferometer* configuration, using a commercial available heterodyne interferometer (Agilent) and performing a simultaneous measurement on the same target.
5. The behavior of the *Delft interferometer* configuration when two coaxial beams from a Zeeman-type laser are applied as the two source frequency inputs.

Appendices

Appendix A.1

The three interferometer measurement systems

The three measurement systems described in this appendix, are build to investigate the performance of two *Delft interferometer* configurations when using fiber delivered source frequencies.

System I Free-space Generalized Delft configuration

The first measurement system using the *Delft Generalized interferometer* configuration is depicted in Figure 7. It has shown to operate with sub-nm measurement uncertainty (*Appendices B.1* and *B.2*) using free-space beam delivery. The next step is to investigate if the same configuration is also able to measure equally accurate when fiber-coupled. The purpose of this system, *System I*, is to reproduce results from previous research (*Appendices B.1* and *B.2*). The new obtained results will function as a reference regarding the results obtained by *System II* (see section next section.
How the heterodyne frequency is generated in this system and how the interferometer is build, will be explained in *Appendix A.2* and *Appendix A.4* respectively.

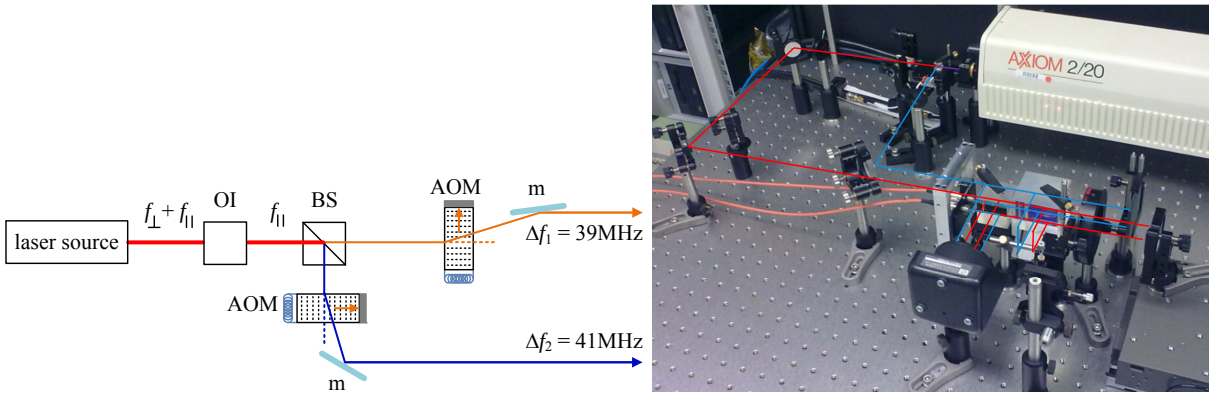

Fig. 7: *Figure 7(a) schematically shows the heterodyne source frequency generation for the free-space system. Figure 7(b) shows that the free-space system uses mirrors for guiding the source frequencies from the Acousto Optical Modulators (AOM's) towards the interferometer, depicted in the photo by the red and blue lines. The configuration seen in the photo is of the* Generalized Delft *type, explained in* Appendix A.4.

System II Fiber coupled Generalized Delft configuration

The configuration of the interferometer itself is equal to the configuration depicted in figure 7, the difference is the method of source frequency delivery to the interferometer. For this transport polarization maintaining single mode fibers (pm-fibers) are used instead of mirrors. The reference interference signal originating from PD_{ref} is used to investigate fiber induced phase-differences.

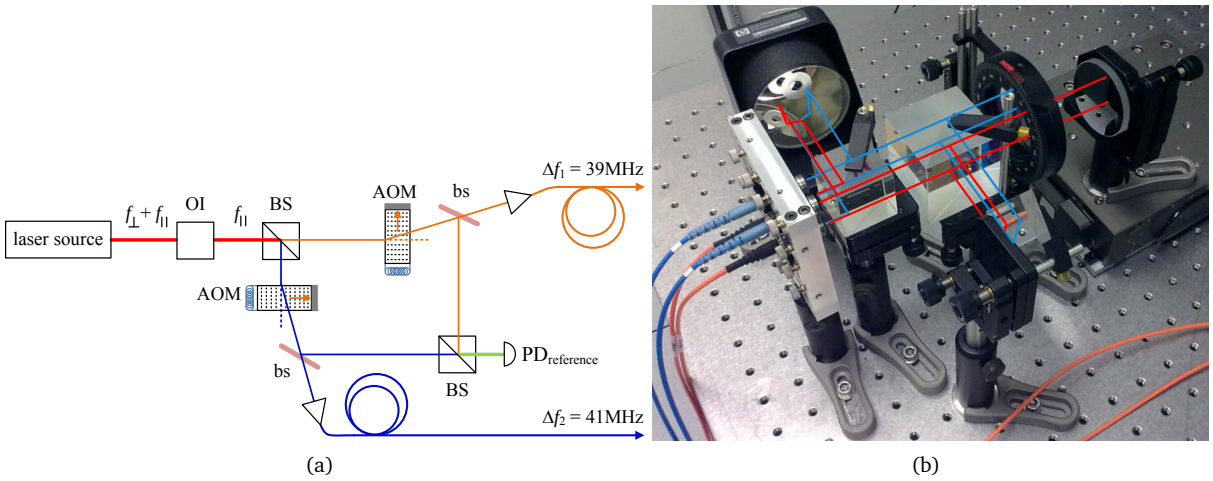

Fig. 8: *Figure 8(a) shows that the heterodyne source frequency generation takes place in the same way as depicted in figure 7(a) except for the generation of a reference signal, PD_{ref} (see the next section). The configuration of the interferometer itself is equal to the interferometer configuration in figure 7(b), except for the difference in the source frequency delivery method. The two blue fibers (at the left in the photo) are the pm-fibers which deliver the source frequencies to the interferometer. The orange multi mode fibers (mm-fibers) transport the generated interference signals from the interferometer to two photodetectors.*

System III Fiber coupled Delft Corner Cube configuration

The third measurement system build, is the *Delft Corner Cube configuration* using fiber-coupled beam delivery by means of mm-fibers. Measurements obtained with this system are discussed in the article of Chapter 2. The means of heterodyne frequency generation is equal to *System II*, except that mm-fibers instead of pm-fibers are applied.

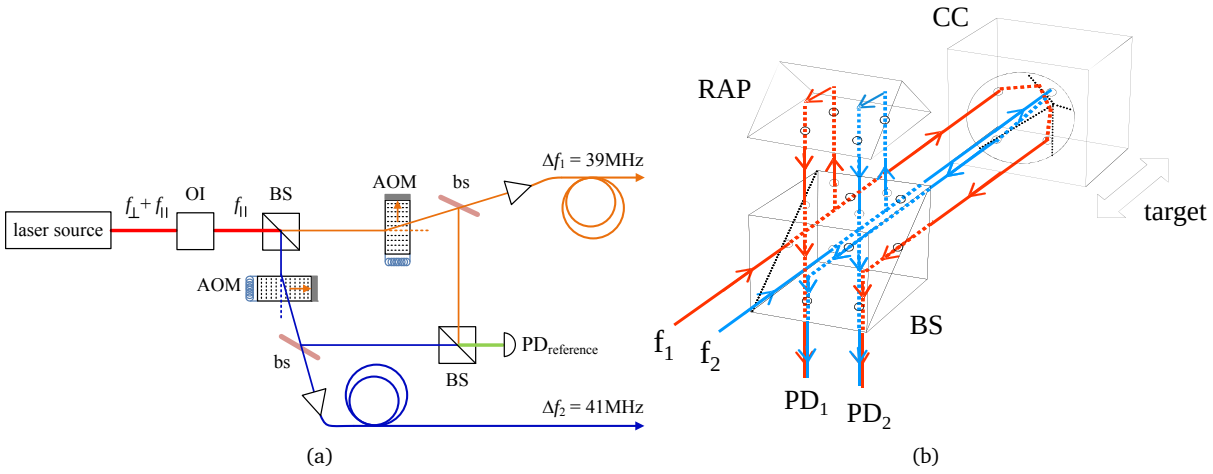

Fig. 9: *The heterodyne source frequency generation in figure 9(a) is equal to the configuration depicted in figure 8(a) but the light exiting the AOM's is now launched into mm-fibers which are not polarization maintaining. Figure 9(b) shows a schematic representation of the the* Delft Corner Cube configuration *which is the most basic type of the* Delft interferometers.

Appendix A.2

Generating heterodyne source frequencies

Now the three different systems which were used for testing have been shown briefly, it is time to elaborate on the generation of the source frequencies. The laser source used for the research is a modified Zygo Axiom 2/20 two mode Helium Neon laser (HeNe-laser). The modifications made to the laser consist of the removal of a polarizer, a beam splitter, two AOM's and a recombination wedge prism. If the laser was not modified, it would operate as following:

Two mode laser light is generated by the laser tube, one of the outgoing modes is blocked by the polarizer depending on its polarization orientation (the two modes originating from the laser have a difference in frequency and polarization orientation). After one frequency has passed the polarizer, the beam splitter splits the beam and divides it 50/50 between two AOM's. Each AOM's shifts the frequency of light to a different frequency, using traveling sound waves inside a crystal (see Figure 11 and text for explanation). The modified light by the AOM's is then be recombined again into a heterodyne coaxial beam, using a recombination wedge prism.

For our investigation this whole light modification process was unwanted since it results in a so called 'non-ideal laser source'. The coaxial heterodyne beam of such a laser allows for polarization and frequency mixing, eventually leading to the presence of 'periodic nonlinear' errors in the measurement output. These components were therefore removed and re-implemented for our research as shown in Figure 10(a). One of the two modes originating from the HeNe-laser is blocked by an Optic Isolator (OI), consisting of a Faraday-rotator. This OI blocks light with a specific polarization orientation while also preventing back reflections from other optical components such as the interferometer. If these back reflections are allowed reenter the laser-tube, they could potentially destabilize the laser source.

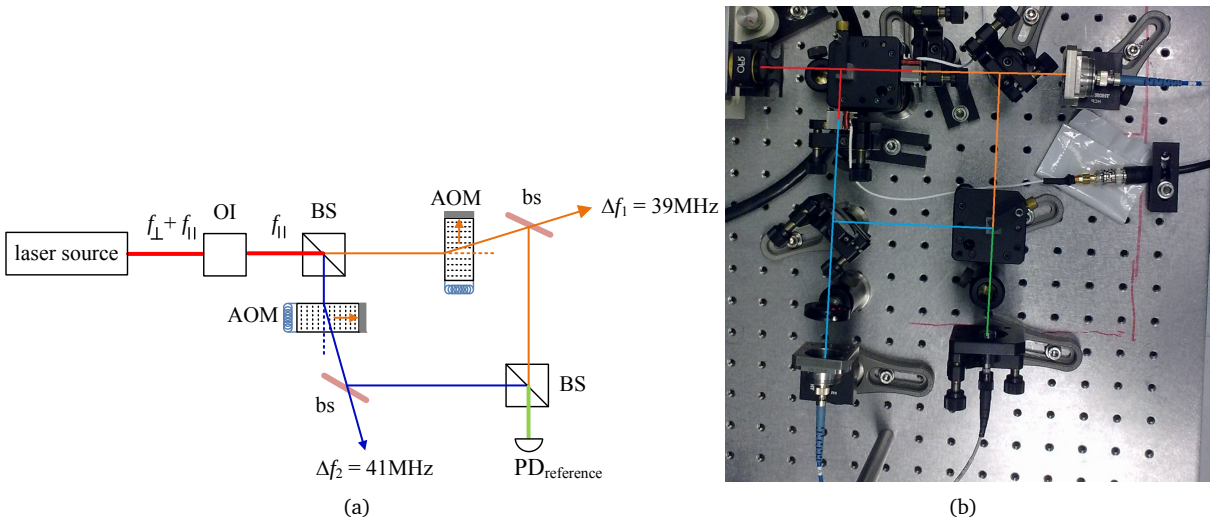

Fig. 10: *A schematic representation of heterodyne frequency generation is shown in figure 10(a). The modified Axiom laser generates two laser modes of which one mode is blocked by an Optical Isolator (OI). After the OI the beam is split 50/50 and transported to two AOM's shifting the frequency of the incoming light. The light exiting from the AOM's first pass a beam sample (bs) which sample 4% of the light before it is launched into the optical fibers. The sampled light is recombined by the right beam splitter (BS), where a 2MHz interference signal is created, acting as a reference. Figure 10(b) shows how the system in 10(a) is realized in reality, the blue fibers located at the bottom-left and top-right are pm-fibers, the bottom-right mm-fiber contains the reference interference signal.*

After the OI we only have light containing one frequency, at half the initial optical power since we blocked one source frequency containing the other half of the power. For operation of a heterodyne interferometer two source frequencies with a certain frequency offset are required. The light exiting the OI is therefore split 50/50 by a neutral beam splitter (non-polarization sensitive) and delivered to two AOM's, one operating at 39MHz and one at 41MHz. This results in a frequency difference of 2MHz between f_1 and f_2

(see also Figure 10(a)). This difference in frequency is the frequency at which interference takes place. From each AOM only the positive first order mode is used, the other optical modes are blocked using an iris.

The reason that two AOM's were used (one operating at 39MHz and one at 41MHz) instead of one AOM operating at 2MHz, is related to practical usage. An operating frequency of 2MHz results in a small angle of exit ('α') between the exiting modes, extraction of a clear single higher order mode is therefore difficult at such 'low' frequencies. The next reason, why there is no frequency offset created between f_1 and f_2 of 40MHz using only one AOM operating at 40MHz, is related to limitations of the phase-measurement equipment. Electronic measurement equipment is required for interpretation of the interference signal, since the offset frequency determines the interference frequency, it would result in a interference signal of 40MHz. This is a far too high frequency for reliable interpretation by the phase-measurement equipment.

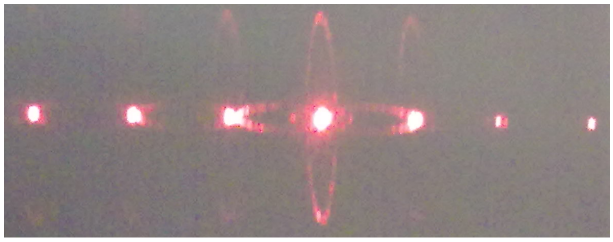

Fig. 11: *The photo shows light exiting from an operating AOM. The zero order mode is the red bright spot in the center, the positive first order mode is the first next spot to the right and the second positive mode is again at the right. The negative modes are located at the left. What can be noticed is that the brightness of the spots differ, the zero order mode contains the most power while the higher modes contain each less optical power. If the operating frequency of the AOM decreases, the modes will exit the AOM at a smaller angle, making it more difficult to obtain a clear single mode signal.*

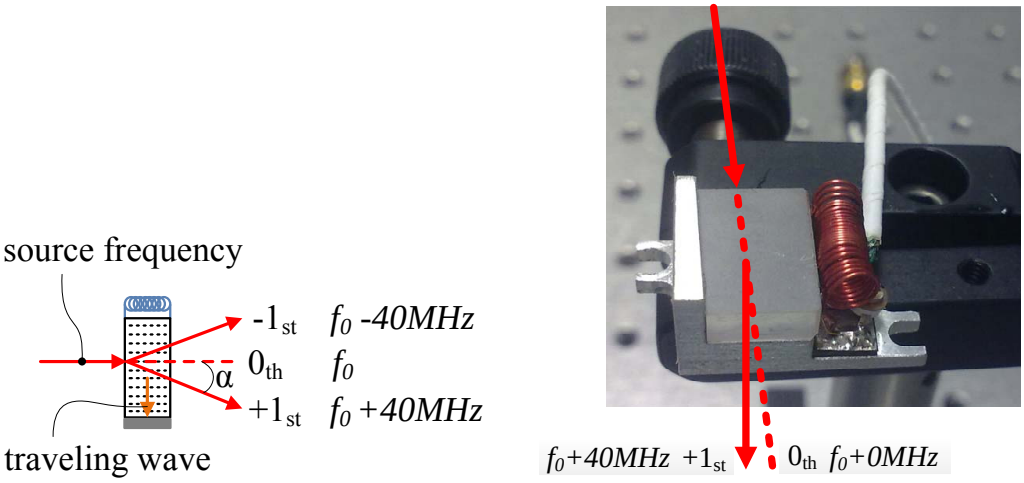

(a) (b)

Fig. 12: *A schematic representation of an AOM can be seen in figure 12(a) showing three modes, the zero order mode contains the unaltered source frequency while the positive first order contains the source frequency plus a frequency offset. The negative first mode results in the source frequency minus the frequency offset. Whether the incoming light is upshifted or downshifted in frequency, is related to the direction of the acoustic traveling wave (orange arrow) through the crystal. A real AOM generates beside the zero and first order modes also higher order modes (see Figure 11). The angle of exit 'α' increases at increased operating frequencies. Figure 12(b) shows how one of the two AOM's used for the research looks in reality. The electronics for attenuation of the crystal are located near the coil at the right side. A diffracted beam exits at an angle that depends on the wavelength of the light relative to the wavelength of the sound inside the crystal as the electronics generate an acoustic traveling wave inside the crystal.*

Appendix A.3

Source frequency delivery

The light passing the two irises is ready to be used, but the light first needs to be transported to the interferometer. This transport either takes place using the free-space method where mirrors guide the light through air or vacuum, shown in Figure 13(a), or transport takes place fiber-coupled, using optical fibers, Figure 13(b). After the irises a part of the light (4%) is extracted by a beam sampler before the light is launched into the fibers. The sampled light is used for creating a phase-reference, this reference will tell us how much the transport method will affect the phase of the transported frequency. The other 96% of the light is available for use by the interferometer.

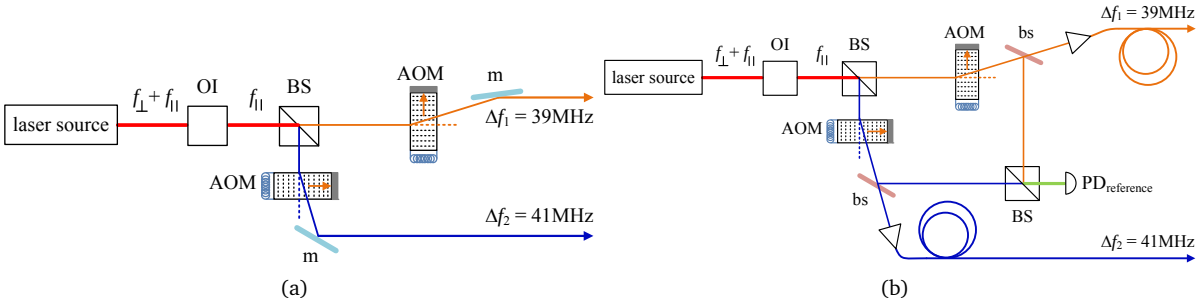

Fig. 13: *Above schemes differ from each other in the method of source frequency transport, in Figure 13(a) mirrors (m) guide the light exiting the AOM's while the in Figure 13(b), fibers are used.*

The mirrors used for guiding light can differ in materials causing reflection, resulting in different absorbtion/reflection ratio's and their shape can vary from concave to flat to convex shapes. The same holds for optical fibers, their core material and size knows a wide variety of types. Fibers having a core size in the order of just a few micrometers are called 'single' mode fibers because they allow only for one optical pathway through their core material, resulting in the transport of 'single mode' light, see Figure 14. Fibers with core sizes up to a few hundred micrometer allow for multiple optical pathways which not necessarily follow the direction of the core axis (see the two top fibers in Figure 14). These fibers are able to transport 'multiple modes' of light and are thus called 'multi mode' fibers. These are the two main types of optical fibers that can be divided into several sub-types, each having its own specific behavior. Single mode fibers are also available in a number of variants as shown in Figure 15, they can be polarization maintaining or non-polarization maintaining.

The difference between the single mode and multi mode fibers is related to the ease in practical use and the optical quality of the transported light. The single mode fiber require tighter alignment tolerances compared to multi mode fibers, caused by the the much smaller core diameter. This high degree of align-

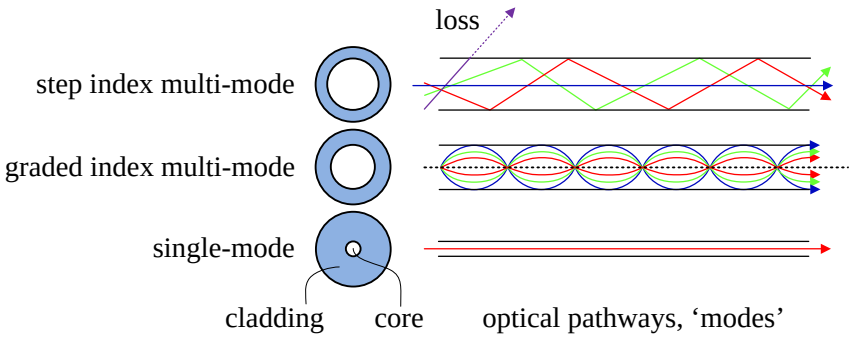

Fig. 14: *There are mainly two different types of fibers that can be distinct, you have the multi mode fibers which allow for multiple optical pathways in their core and you have the single mode fibers which allow for only one optical pathway, schematically shown in the Figure. The fibers differ in core diameter and material.*

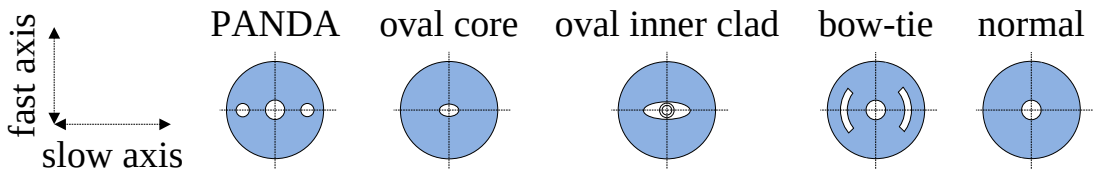

Fig. 15: *In the above schematic the cross-sectional geometry of five single mode fibers are depicted. The 'normal' fiber is non-polarization sensitive and will show a time varying polarization state. The other four fibers are polarization sensitive due to the anisotropic refractive index of their core material. The vertical axis and horizontal axis differ in refractive index, also called the 'fast' and 'slow' axis, resulting in sustaining a polarization state.*

ment makes it difficult to align with the incoming beam of light and obtaining a high efficiency optical coupling. The result of using single mode fibers is their higher quality delivered light, compared to multi mode fibers.
Using polarization maintaining single mode fibers will result in the best optical output quality but it is also the type of fiber that requires the highest degree of alignment since it is also polarization sensitive.

Polarization maintaining multi mode fibers were used for source frequency delivery of System II (see *Appendix A.1*). The purpose of this measurement system was to see if this system could measure with sub-nm uncertainty when fiber coupled delivery is applied. High optical output quality was required to eliminate as much error sources as possible.

The third system was equipped with graded index multi mode fibers, to investigate whether it is possible to measure with sub-nm uncertainty having a much lower light quality. The lower quality light output is dominated by a time varying polarization state, multiple optical modes and a deformed wave front. These phenomena are not present in polarization maintaining single mode fibers. But, multi mode fibers are more practical to handle since they require less alignment, making them more suitable for application in a modular system where 'plug-and-play' behavior is aimed for.

What can be noted is that there is a relation between output quality and the required alignment tolerances. Tight alignment tolerances require much effort to install the fiber but will eventually result in highly conditioned optical output. It also works the other way, easy installation results in less well conditioned optical output.

Appendix A.4

The 'Generalized' and 'Corner Cube' interferometer configurations

Till so far the laser source, the modification of the heterodyne source frequencies and the method of transport of these frequencies towards the *Delft interferometers* have been discussed. The interferometer itself is the unit responsible for guiding and interfering the source frequencies, related to displacement of a target. Two different configurations of interferometers were used for the measurements described in the two articles in *Chapter 1* and *Chapter 2*. Both configurations are based upon the same concept: spatially separated source frequency pathways and double detection.

The main reason for using the spatially separated optical pathways is to eliminate the 'periodic error'. This type of error can be found in many heterodyne interferometer configurations due to 'polarization crosstalk' between the two source frequencies. This crosstalk leads to frequency mixing, causing a periodic nonlinearity to appear in the system. This error needs to be eliminated or decreased in size if sub-nm measurement uncertainty is wanted. In typical heterodyne interferometers that measure in aerial environments, the dominating error source is not the periodic error but the time variant air refractive index (also other types of gaseous medium will show the same behavior). The time varying refractive index error is not present in systems operating in a vacuum environment due to the absence of a gaseous medium. In this type of operating environment it is the periodic error that becomes the governing error source. This appendix describes how the *Delft interferometer* designs eliminate the periodic error.

Corner Cube configuration

This *Delft interferometer* configuration uses a corner cube as target, figure16, and is therefore called the *Delft Corner Cube configuration* (also the *Delft-CC configuration*). It is the most basic configuration and consists of the minimum required optical components. The aim of this configuration is the elimination of the periodic nonlinearity by using spatially separated optical pathways throughout the whole interferometer until the final interfering surface.

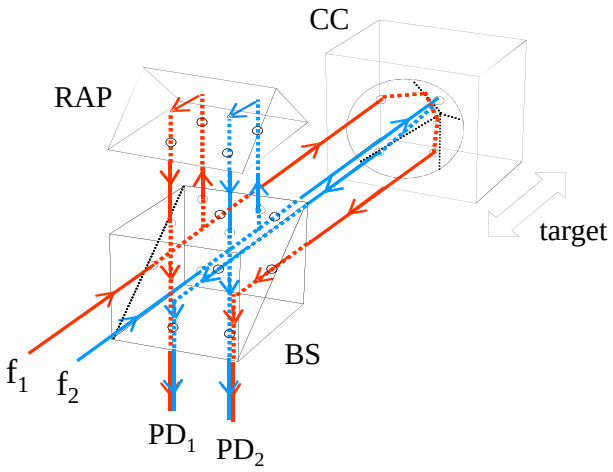

Fig. 16: *The* Delft Corner Cube configuration *is the most basic variant of the* Delft interferometers*. It consists of only three optical components for creating interference signals. The two source frequencies are injected at the left into the interferometer and are first split by a non polarization sensitive beamsplitter (BS). The 50% which is reflected into the Right Angle Prism (RAP) is reflected back into the beam splitter and reaches the two photodectors PD_1 and PD_2, acting as a reference. The other 50% travels forth and back a Corner Cube (CC) where it is translated diagonally. This way each photodetector receives both frequencies.*

Figure 16 shows the *Delft Corner Cube configuration*, receiving the two source frequencies f_1 and f_2 from the left. They both are split 50/50 by a neutral beamsplitter (BS) of which one portion travels towards

a Right Angle Prism (RAP) while the other portion travels towards the target, a Corner Cube (CC). The portion traveling to the RAP functions as a reference and is reflected back into the beamsplitter to eventually hit the photodetectors, PD_1 and PD_2. The light traveling towards to the CC is translated diagonally and then reflected back into the beamsplitter to finally also hit the photodetectors. This way photodetector PD_1 receives f_1 as reference and f_2 containing target displacement information. Photodetector PD_2 on the other hand, will receive f_2 as reference and f_1 containing target displacement information. A differential measurement is applied between the interference signals detected by the two photodetectors. This is a very valuable methods of signal processing since it will cancel out fiber induced phase shifts.

In this configuration the light reflects off the target only once, meaning that if the target moves one unit, the optical pathway is lengthened by two units. During the target displacement one of the photodetectors will measure a positive phase shift while the other detector measures a negative phase shift. Subtracting these signals properly will result in an increase of a factor four in resolution (if the target displaces one unit we measure four units).

Generalized configuration

The *Delft Generalized configuration* shown in Figure 17, is an update of the *Delft-CC configuration*. In the figure can be seen that the source frequencies are delivered at the left and first are split by a neutral beamsplitter (BS), equal to the *Delft-CC configuration*. The first 50% is again used for creating a reference signal and is travels through a Right Angle Prism (RAP) before it is reflected into the photodetectors (PD_1 and PD_2) via the beamsplitter. The other 50% continues its travel towards a polarization sensitive beamsplitter (PBS) which is fully transmissive for the initial polarization state of the incoming light. After the light passes the PBS, it will meet a Quarter Wave Plate (QWP) where the polarization orientation is rotated 45^o [3]. The light then meets two mirrors, a reference mirror (Mr) and a measurement mirror (Mm) which acts as our moving target (see *Appendix A.5*). The light reflected off these two mirrors pass the QWP for a second time and is now rotated 45^o for a second time, resulting in a total rotation of 90^o with respect to the original orientation. Due to this new polarization orientation, the light will not be transmitted but reflected by the PBS into a Corner Cube (CC). The light is then reflected back into the PBS after it is diagonally mirrored by the CC. The PBS reflects the light into the QWP for a third time (rotating the polarization orientation to a total of 135^o) and after reflection from the two mirrors, the light passes the QWP for a fourth time. At this stage, the new polarization orientation with respect to the original incoming light has been rotated 180^o. The PBS has now become again transmissive for the light and allows the light finally to reach the photodetectors to interfere with the reference light, creating the 'beat signal' containing the target its displacement information.

The basic operation of this configuration is equal to the *Delft-CC configuration* but it is a more complicated system, offering some advantages. In the *Delft-CC configuration* the light reflects off the target only once, lengthening the optical pathway by two units. In this *Generalized Delft configuration*, the light reflects off the target and reference mirror twice (due to the PBS and the QWP), resulting in an optical resolution of a factor of four (instead of two with the *Delft-CC configuration*). If then also a differential measurement between PD_1 and PD_2 is performed, the resulting resolution will be twice the resolution of the *Delft-CC configuration*.
Measuring at increased resolution is useful for sub-nm accurate measurements but it also reveals the presence of the periodic nonlinearity, even if it is small. That is one of the reasons for putting together this theoretically 'periodic error free' configuration.
Another feature of this design is the use of the reference mirror (Mr) acting as a thermal datum if the optical components are all attached (i.e. glued) together. This reference mirror automatically adapts the optical pathway if the monolithic block deforms due to thermal loads, correcting for a part of the deathpath error.

[3] This rotation is not a 'true' rotation, a QWP causes a phase difference which alters the polarization state. Saying that the light is rotated 45^o after passing a QWP is a more simple theoretical replacement of what actual takes place with the polarization of the light. Though speaking of polarization rotation in degrees is not fully correct, it is sufficient to understand its operation in our case.

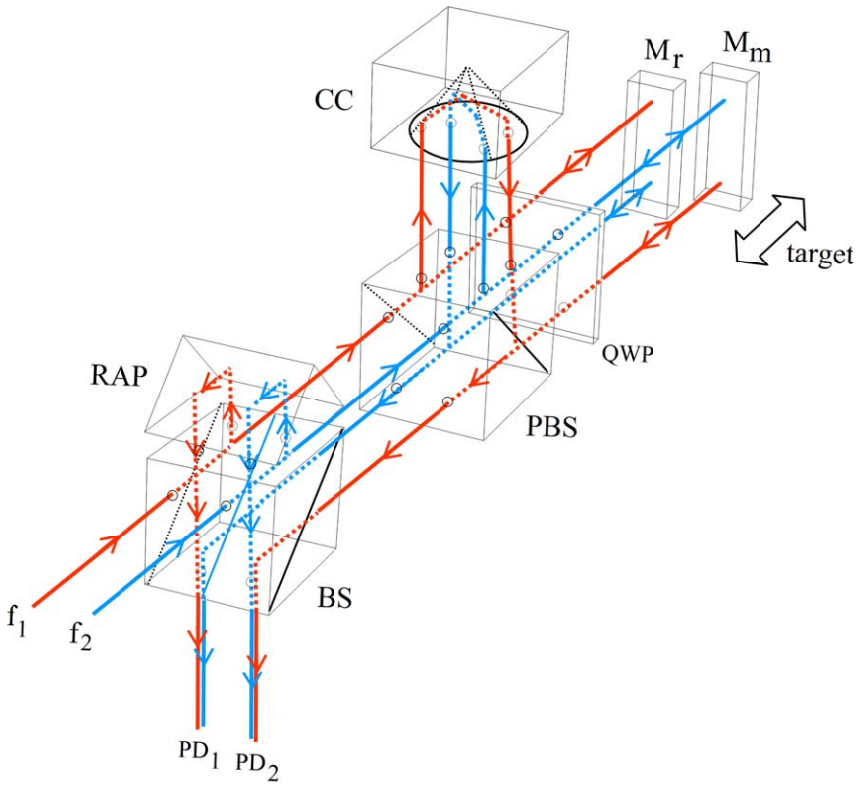

Fig. 17: *The number of optical components of this configuration is larger than that of the* Delft-CC configuration *but it will result in a twofold of the measurement resolution while the basics stay the same. Another feature in this design is that the reference mirror (Mr) in this configuration could serve as a thermal datum for the interferometric block when constructed as a monolith.*

Appendix A.5

The measurement targets

The aim of the total research described in this report, is to design an interferometric measurement system for use in a host-system such as a lithography machine. Inside this system the interferometer(s) will be used for tracking targets such as a wafer carrying chuck or the reticle stage. For our research we do not have a 'real' chuck or reticle stage at our disposal, that is also not necessary. As target replacement we have implemented an Aerotech air bearing stage in our lab, having one Degree Of Freedom (DOF). The stage is computer controlled and can execute movement according a predetermined program (i.e. displacement-, velocity- and acceleration profiles). The stage is a so called 'linear' stage and is driven by a linear electric motor.

High quality mirrors are normally attached at the locations where the light of the interferometer(s) 'touch' the target. As substitution of the high quality mirrors, we equipped the air bearing stage with either a Corner Cube reflector fig.18(a), or a plane mirror 18(b) depending on the interferometer configuration. The movement of this mirror/reflector is our target movement which is measured by the interferometer with sub-nm uncertainty.

If measurement errors show up, you don't know if they originate from the movement of the stage or from the measurement system itself. A number of measurements were therefore performed with the stage driving the target at different constant velocities. This way it is possible to distinct stage vibration errors from systematic measurement system errors.

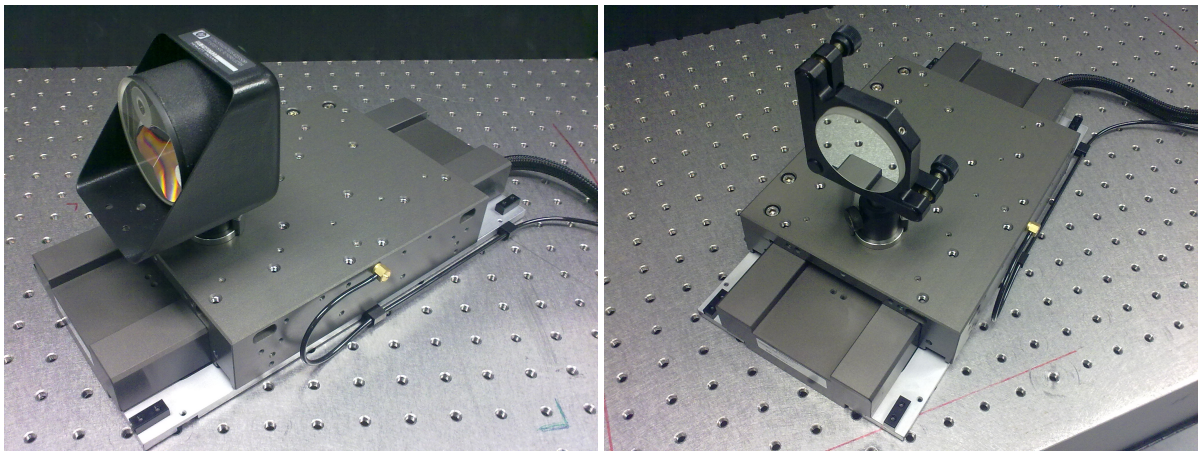

(a) (b)

Fig. 18: *The computer controlled air bearing stage implemented in our lab carries a target forward and backwards with one DOF. The stage is equipped with a corner cube reflector,18(a) or a plane mirror 18(b), located on the top of the stage acting as a target when the stage moves. The relative displacement of this 'target' is measured by the interferometer.*

Appendix B.1

Article:
Simple hetrodyne laser interferometer with subnanometer periodic errors

In this article from the scientific journal: *Optics Letters*, the *periodic error* free operation of the *Delft Corner Cube* interferometer design is described. It's one of the first articles about the operation of this type interferometer.

Simple heterodyne laser interferometer with subnanometer periodic errors

Ki-Nam Joo,[1,*] Jonathan D. Ellis,[1] Jo W. Spronck,[1] Paul J. M. van Kan,[2] and Robert H. Munnig Schmidt[1]

[1]*Mechatronic System Design, Department of Precision and Microsystems Engineering, Delft University of Technology, Delft, The Netherlands*
[2]*NMi Van Swinden Laboratorium BV, Delft, The Netherlands*
**Corresponding author: k.joo@tudelft.nl*

Received October 9, 2008; revised December 10, 2008; accepted December 11, 2008; posted January 6, 2009 (Doc. ID 102595); published January 30, 2009

We describe a simple heterodyne laser interferometer that has subnanometer periodic errors and is applicable to industrial fields. Two spatially separated beams can reduce the periodic errors, and the use of a right-angle prism makes the optical configuration much simpler than previous interferometers. Moreover, the optical resolution can be enhanced by a factor of 2, because the phase change direction is opposite between reference and measurement signals. Experiments have demonstrated the periodic errors are less than 0.15 nm owing to the frequency mixing of the optical source. The improvements for reducing the frequency mixing of the optical system are also discussed. © 2009 Optical Society of America

OCIS codes: 120.3180, 120.3930, 120.3940.

The periodic errors limit the accuracy of heterodyne laser interferometers because they deteriorate the purity of the interference signals [1]. Since the periodic errors of the laser interferometers were first predicted [2], research pertaining to theoretical models and compensation techniques has been investigated and reported [3–5]. Recently, a real-time first-order periodic error correction technique was validated under various experimental conditions indicating that the remaining periodic error is at the subnanometer level [6]. In addition to compensation methods, nonpolarizing optical configurations to eliminate the periodic errors have been designed [7–9]. The common feature of these interferometers is to use spatially separated beams that have different frequency components. Essentially, the polarization states are never mixed; thus the nonlinearity can be significantly reduced. However, the optical setups are complicated because both beams propagate separately, which requires additional optical components [7]. Although several designs have been reported with heterodyne interferometers using an acousto-optic frequency shifter (AOFS) as a beam splitter [8,9], the small AOFS diffraction angle and their specific configurations limit the applicability for displacement measurements.

In this research, a simple and industry-adaptable heterodyne laser interferometer designed to significantly reduce periodic errors is proposed and tested. The periodic errors are essentially caused by splitting and recombining two nonideal beams using polarizing optics that are both nonideal and are sensitive to alignment. To eliminate the periodic errors in the optical configuration, two beams with different optical frequencies should be spatially separated to avoid the frequency and polarization mixing.

Figure 1 shows the optical configuration that was employed in this investigation. An optical source provides two parallel beams to the interferometer, where each beam has the same polarization state but has different optical frequencies f_0 and f_0+f_s, respectively. The two beams propagate to a nonpolarizing beam splitter (NPBS) where they are split into two sets of beams, reference and measurement beams. The reference beams are reflected by a right-angle prism (RAP), and the measurement beams are reflected by a retroreflector (RR). The RR provides symmetry with respect to a central point and causes the measurement beams to cross each other. The reference beams, on the other hand, have the line symmetry by the RAP. Each set of beams travels back to the NPBS and is recombined to create two beat signals with the frequency of f_s, which are detected by the photodetectors, PD_1 and PD_2.

While the RR is moving the measurement beams are phase shifted, caused by the Doppler frequency shift, and are measured by PD_1 and PD_2. In this case, the heterodyne signals from the photodetectors provide the same amplitude, but the phase shift direction is in the opposite direction between the two signals. Thus the two interference signals from PD_1 and PD_2 can be expressed by $\cos(2\pi f_s t - 2k\Delta L)$ and $\cos(2\pi f_s t + 2k\Delta L)$, respectively, where k is the wavenumber and ΔL is the displacement of the target RR

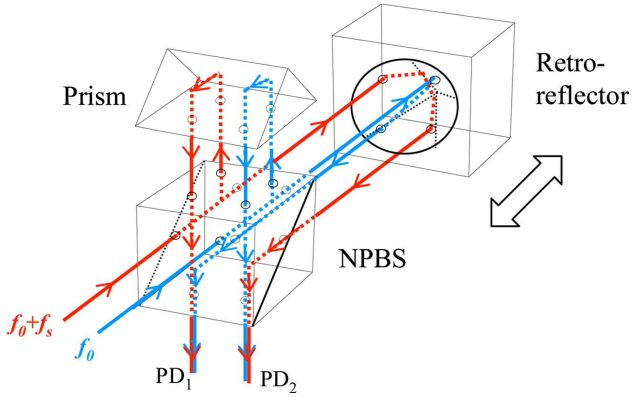

Fig. 1. (Color online) Proposed optical configuration of a heterodyne laser interferometer to reduce the periodic errors. NPBS, nonpolarizing beam splitter; PD_1, PD_2, photodetectors.

0146-9592/09/030386-3/$15.00 © 2009 Optical Society of America

while it is moving. When the phase difference between the signals from PD_1 and PD_2 is measured, the total phase difference is $4k\Delta L$, which is an effective optical resolution of four. The beams are spatially separated, and the optical paths are not overlapped in the interferometer; therefore no leakage of light is detected except ghost reflections. It should be noted that ghost reflections can be minimized by proper antireflection coatings and alignment techniques. Moreover, polarizing optics, which can generate the frequency and/or polarization mixing, are not used. This interferometer is totally insensitive to the misalignment of optical components, although careful attention is required in the initial alignment owing to the prism.

To validate the effectiveness of the proposed interferometer, we performed feasibility experiments with a commercial heterodyne laser (Axiom 7701, Zygo Corp.) as an optical source, as shown in Fig. 2. The coaxial beams of the heterodyne laser are split into two beams, f_1 and f_2 ($f_2-f_1=20$ MHz), by a polarizing beam splitter (PBS), and the f_1 beam passes through another AOFS, which induces the frequency shift, δf, of 19.9 MHz. The diffracted beam ($f_1+\delta f$) and the reflected beam (f_2) by the PBS are adjusted to be parallel by mirrors and have the same polarization state after a polarizer. The final heterodyne frequency split, $f_2-(f_1+\delta f)$, is approximately 100 kHz. Although the leakage frequency component of each beam is not completely removed from the schematic in Fig. 2, the leakage ratio can be significantly reduced. The two beams can be expressed as

$$E_1 = \exp[j(2\pi f_2 t)] + \varepsilon_1 \exp[j(2\pi f_1 t\ ],$$

$$E_2 = \exp[j(2\pi(f_1 + \delta f)t\ ] + \varepsilon_1 \exp[j(2\pi(f_2 + \delta f)t)] + \varepsilon_2 \exp[j(2\pi f_1 t)] + \varepsilon_1\varepsilon_2 \exp[j(2\pi f_2 t)], \quad (1)$$

where ε_1 is the leakage ratio from the laser and the

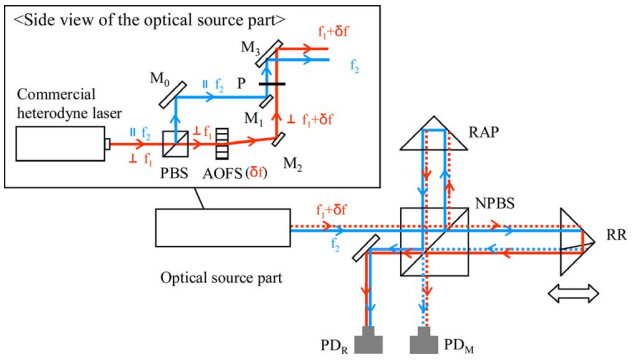

Fig. 2. (Color online) Experimental setup. AOFS, acousto-optic frequency shifter; M_0, M_1, M_2, M_3, angle-adjusted mirrors; NPBS, nonpolarizing beam splitter; RAP, right-angle prism; RR, retroreflector; PD_R, PD_M, reference and measurement photodetectors; PBS, polarizing beam splitter; P, polarizer. The inlet is the configuration of the optical source with two spatially separated beams on the side view. Note that the solid line is the spatially upper beam, and the dotted line is the lower beam.

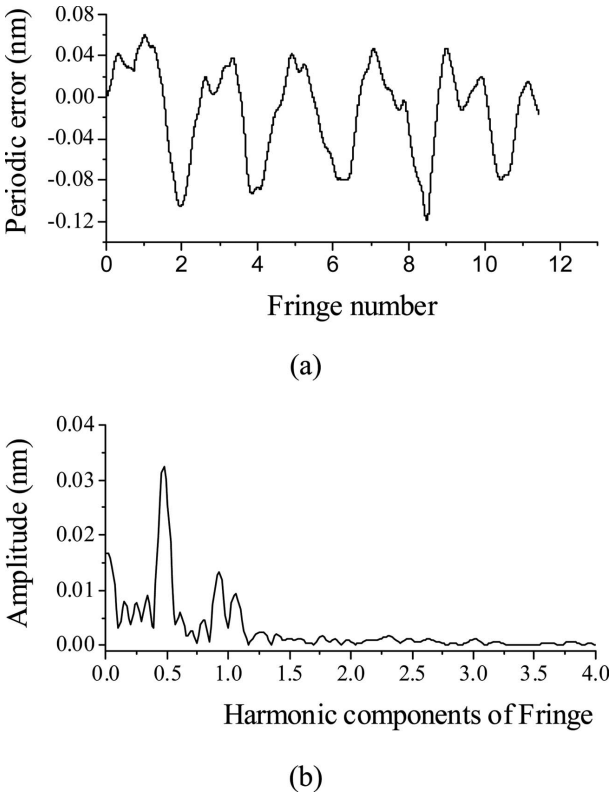

Fig. 3. Experimental result of the periodic error from the phase quadrature measurement method and (b) Fourier transformed result of the periodic errors (a). The main error is caused by the frequency mixing of the optical source and other noises are from ghost reflections and electronics.

PBS, and ε_2 is the leakage ratio of the AOFS. In Eq. (1) and [7], the leakage term causing the phase error is $\varepsilon_1\varepsilon_2 \exp[j(2\pi f_2 t)]$ and the phase error ($d\phi$) and the amplitude change (dR/R) are expressed from the phase quadrature measurement method in [7] as

$$d\phi = 2\varepsilon_1\varepsilon_2 \sin(2k\Delta L),$$

$$\frac{dR}{R} = 2\varepsilon_1\varepsilon_2 \cos(2k\Delta L). \quad (2)$$

From Eq. (2), the phase error is correlated with the amplitude change and the periodic error cycles at half the fringe frequency because the measured phase is $4k\Delta L$. Figure 3 shows the measurement results of the periodic error in the system and the Fourier transformed result. The amplitude and the phase were measured by a commercial lock-in amplifier (5210, Signal Recovery), while the RR was moved by a piezoelectric stage. The overall periodic errors were calculated using Eq. (2) to be estimated below 0.15 nm in Fig. 3(a), and the dominant periodic error was caused by the ratios ε_1 and ε_2 with half the period frequency and the amplitude of ±33 pm in Fig. 3(b). The sources of remaining peaks with the period frequency in Fig. 3(b) are from the parasitic reflection of the optical components and electrical demodulation noise.

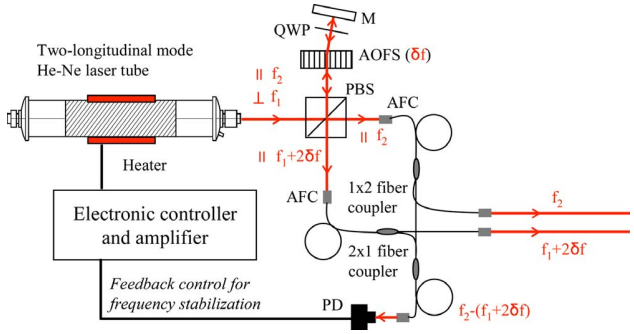

Fig. 4. (Color online) Proposed optical source to obtain a frequency-stabilized laser with two parallel beams to reduce frequency mixing. PBS, polarizing beam splitter; AOFS, acousto-optic frequency shifter; QWP, quarter-wave plate; M, mirror; AFC, angled fiber coupler; PD, photodetector.

To fully verify the theoretical elimination of periodic errors, the laser source must be free from frequency mixing. Employing two AOFSs with different frequency shifts has been shown to remove the frequency mixing [7]. This laser system, however, increases the overall cost, which is not desirable for both research and industrial fields. A frequency-stabilized and an offset-locked laser set is another potential alternative to improve the performance of the interferometer, although the phase jitter noise between the two lasers remains [10].

An alternative scheme to obtain two parallel beams with minimal frequency mixing is shown in Fig. 4. The laser source is a two-longitudinal mode He–Ne laser tube that has approximately 600 MHz frequency difference, f_2-f_1, and orthogonal polarization states. This initial beam is split into two by a PBS and the reflected beam, f_1, passes through a polarization sensitive AOFS ($\delta f \sim 300$ MHz), where the diffracted beam is orthogonally polarized to the input beam. It is reflected by a mirror passing through a quarter-wave-plate (QWP) twice and then back through the AOFS. This beam then passes through the initial PBS and into a fiber coupler. Even though the leakage beam reflected by the PBS goes back to the laser tube, the laser stabilization is not affected owing to the shifted optical frequency [9]. The second beam from the source, f_2, passes through the initial PBS and into a fiber coupler. Two fiber splitters are used, and one arm from each set is combined with a second into one fiber coupler to recombine the beams to provide feedback control to obtain a stabilized frequency. The heterodyne frequency is then $f_2-(f_1+2\delta f)$, and it is used for frequency stabilization. The orthogonality of the two longitudinal modes, polarization characteristic of the AOFS and passing through the AOFS twice, should reduce the ratio of leakage frequency components.

To summarize, a simple heterodyne laser interferometer was proposed to remove the periodic error inherent to laser interferometers. The reference and measurement beams are spatially separated to prevent any frequency mixing, and the use of a right-angle prism makes it possible to construct a simple interferometer setup and enhance the optical resolution by a factor of 2. Experimental results showed the periodic error to be less than 0.15 nm, which was dominated by the frequency mixing of the optical source. Several options for alternative optical sources to reduce the frequency mixing were also proposed and discussed.

This work was supported by the Dutch Innovatiegerichte Onderzoeksprogramma's (project 04001) and NMi in the Netherlands. The authors thank Eric Buice for his comments on this review.

References

1. N. Bobroff, Meas. Sci. Technol. **4**, 907 (1993).
2. R. C. Quenelle, Hewlett-Packard J. **34**, 10 (1983).
3. W. Hou and G. Wilkening, Precis. Eng. **14**, 91 (1992).
4. T. Eom, T. Choi, K. Lee, H. Choi, and S. Lee, Meas. Sci. Technol. **13**, 222 (2002).
5. S. J. A. G. Cosijns, H. Haitjema, and P. H. J. Schellekens, Precis. Eng. **26**, 448 (2002).
6. T. L. Schmitz, D. Chu, and L. Hoouck III, Meas. Sci. Technol. **17**, 3195 (2006).
7. C. Wu, J. Lawall, and R. D. Deslattes, Appl. Opt. **38**, 4089 (1999).
8. T. L. Schmitz and J. F. Beckwith, J. Mod. Opt. **49**, 2105 (2002).
9. J. Lawall and E. Kessler, Rev. Sci. Instrum. **71**, 2669 (2000).
10. J. Lawall and J. M. Pedulla, Rev. Sci. Instrum. **72**, 2879 (2001).

Appendix B.2

Article:
Simple heterodyne laser interferometer with subnanometer periodic errors

This second article, published in the scientific journal of optics: *Optics Express*, the operation of the *Generalized Delft* interferometer is explained and discussed.

High resolution heterodyne interferometer without detectable periodic nonlinearity

Ki-Nam Joo*, Jonathan D. Ellis, Eric S. Buice, Jo W. Spronck and Robert H. Munnig Schmidt

Mechatronic System Design, Department of Precision and Microsystems Engineering, Delft University of Technology, Delft, The Netherlands
**k.joo@tudelft.nl*

Abstract: A high resolution heterodyne laser interferometer without periodic nonlinearity for linear displacement measurements is described. It uses two spatially separated beams with an offset frequency and an interferometer configuration which has no mixed states to prevent polarization mixing. In this research, a simple interferometer configuration for both retroreflector and plane mirror targets which are both applicable to industrial applications was developed. Experimental results show there is no detectable periodic nonlinearity for both of the retro-reflector interferometer and plane mirror interferometer to the noise level of 20 pm. Additionally, the optical configuration has the benefit of doubling the measurement resolution when compared to its respective traditional counterparts. Because of non-symmetry in the plane mirror interferometer, a differential plane mirror interferometer to reduce the thermal error is also discussed.

©2010 Optical Society of America

OCIS codes: (120.0120) Instrumentation, measurement, and metrology; (120.3180) Interferometry; (120.3940) Metrology.

References and links

1. W. T. Estler, "High-accuracy displacement interferometry in air," Appl. Opt. **24**(6), 808–815 (1985).
2. H. Bosse, and G. Wilkening, "Developments at PTB in nanometrology for support of the semiconductor industry," Meas. Sci. Technol. **16**(11), 2155–2166 (2005).
3. N. Bobroff, "Recent advances in displacement measuring interferometry," Meas. Sci. Technol. **4**(9), 907–926 (1993).
4. F. C. Demarest, "High-resolution, high-speed, low data age uncertainty, heterodyne displacement measuring interferometer electronics," Meas. Sci. Technol. **9**(7), 1024–1030 (1998).
5. R. C. Quenelle, "Nonlinearity in interferometer measurements," Hewlett Packard J. **34**, 10 (1983).
6. W. Hou, and G. Wilkening, "Investigation and compensation of the nonlinearity of heterodyne interferometers," Precis. Eng. **14**(2), 91–98 (1992).
7. S. J. A. G. Cosijns, H. Haitjema, and P. H. J. Schellekens, "Modeling and verifying non-linearities in heterodyne displacement interferometry," Precis. Eng. **26**(4), 448–455 (2002).
8. V. G. Badami, and S. R. Patterson, "A frequency domain method for the measurement of nonlinearity in heterodyne interferometry," Precis. Eng. **24**(1), 41–49 (2000).
9. T. Eom, T. Choi, K. Lee, H. Choi, and S. Lee, "A simple method for the compensation of the nonlinearity in the heterodyne interferometer," Meas. Sci. Technol. **13**(2), 222–225 (2002).
10. H. Haitjema, S. J. A. G. Cosijns, N. J. J. Roset, M. J. Jansen, and P. H. J. Schellekens, "Improving a commercially available heterodyne laser interferometer to sub-nm uncertainty," Proc. SPIE, 347–354 (2003).
11. D. Chu, and A. Ray, "Nonlinearity measurement and correction of metrology data from an interferometer system," Proc. of 4th euspen Int. Conf., 300–301 (2004).
12. T. L. Schmitz, D. Chu, and L. Houck III, "First-order periodic error correction: validation for constant and non-constant velocities with variable error magnitudes," Meas. Sci. Technol. **17**(12), 3195–3203 (2006).
13. M. Tanaka, T. Yamagami, and K. Nakayama, "Linear interpolation of periodic error in a heterodyne laser interferometer at subnanometer levels (dimension measurement)," IEEE Trans. Instrum. Meas. **38**(2), 552–554 (1989).
14. C. M. Wu, J. Lawall, and R. D. Deslattes, "Heterodyne interferometer with subatomic periodic nonlinearity," Appl. Opt. **38**(19), 4089–4094 (1999).
15. J. Lawall, and E. Kessler, "Michelson interferometry with 10 pm accuracy," Rev. Sci. Instrum. **71**(7), 2669–2676 (2000).
16. T. L. Schmitz, and J. F. Beckwith, "Acousto-optic displacement-measuring interferometer: a new heterodyne interferometer with Anstrom-level periodic error," J. Mod. Opt. **49**(13), 2105–2114 (2002).

#117076 - $15.00 USD Received 11 Sep 2009; revised 21 Dec 2009; accepted 23 Dec 2009; published 8 Jan 2010
(C) 2010 OSA

17. K.-N. Joo, J. D. Ellis, J. W. Spronck, P. J. M. van Kan, and R. H. M. Schmidt, "Simple heterodyne laser interferometer with subnanometer periodic errors," Opt. Lett. **34**(3), 386–388 (2009).

1. Introduction

Since the Doppler frequency shift measurement technology using a two-frequency source was invented in the 1970s, heterodyne laser interferometry has been widely used as an accurate positioning sensor to measure displacements of precision stages [1]. The heterodyne laser interferometer has also been widely used to calibrate other measurement tools such as capacitive sensors, inductive sensors, and optical encoders because of its high dynamic range, high signal-to-noise ratio, and direct traceability to the length standards [2]. Subnanometer level measurements must be achieved to satisfy industrial demands on performance [3]. The rapid development of electronic phase measuring technology made it possible to measure subnanometer displacements in combination with optical resolution determined by interferometer configurations. When a HeNe laser (λ=632.8 nm) is used as an optical source, a commercial displacement interferometer with retro-reflectors, which has the optical resolution of $\lambda/2$ (316.4 nm), can achieve displacement measurements with a $\lambda/2048$ (0.31 nm) resolution from fringe interpolation [4]. The phase measuring electronics, however, introduce a measurement error caused by periodic nonlinearities in the interferometer which deteriorates the purity of the interference signals [3].

From previous research [5–7], it is clear the periodic nonlinearity originates from a mixed heterodyne source and non-perfect polarizing optics. Because a two frequency, orthogonally polarized source is used, there will be non-orthogonality errors and slightly elliptical beams which contribute errors. These combined with imperfect polarizing optics, polarization alignment between the source and optics, ghost reflections, and electronic nonlinearity all created additional nonlinearity errors [3]. Small leakage components from these invoke an unexpected phase change between reference and measurement signals. When the geometrical errors are minimized, periodic nonlinearity is the fundamental error source limiting the implementation of subnanometer displacement measurements. This assumes the measurement is performed in an ideal environment, such as in vacuum, or when the measurement length minimized so the refractive index effects are minimal.

Reducing errors from periodic nonlinearity has been the subject of much research, which can be categorized as either algorithm methods [8–12] or two spatially separated beam interferometer configurations [13–17]. The reduction method algorithms ensure a periodic nonlinearity below 1 nm without changes to the interferometer configuration; however, they require the calibration and additional calculation time. On the other hand, real time reductions can be implemented with modified interferometer setups using two spatially separated beams. The only limitation of these interferometer configurations is their special and often complicated configurations which limit their applicability in industrial and scientific fields.

In this research, we describe two simple heterodyne interferometer configurations, with a retroreflector and with a plane mirror, with two spatially separated beams to eliminate the periodic nonlinearity. These interferometers have a minimum number of optical components and the opposite phase shift direction between interference signals enhances the optical resolution by a factor of two. This optical resolution enhancement allows for simpler optical configurations while achieving the same optical resolution by increasing the number of beam paths in the interferometer.

2. Simple retroreflector interferometer without periodic nonlinearities

Figure 1 shows the heterodyne laser source and retro-reflector interferometer configuration. Because the periodic nonlinearity initially comes from the heterodyne laser source, which has polarization and frequency mixing, two acousto-optic frequency shifters ($AOFS_1$, $AOFS_2$) to generate two different frequencies, ($f_0+\delta f_1$) and ($f_0+\delta f_2$), from a stabilized single frequency (f_0) source were used. By doing so, a beat frequency of ($\delta f_2-\delta f_1$) is created and each beam has no leakage component to cause periodic nonlinearities [14]. The original beams with f_0 from $AOFS_1$ and $AOFS_2$ were blocked with pinholes (PH), which were approximately 200 mm

#117076 - $15.00 USD Received 11 Sep 2009; revised 21 Dec 2009; accepted 23 Dec 2009; published 8 Jan 2010
(C) 2010 OSA

apart from the AOFSs. These two beams from the source part were adjusted and aligned with three mirrors to ensure two separated, parallel beams before entering the interferometer as illustrated in Fig. 1.

The interferometer, as depicted in the upper portion of Fig. 1, consists of a beam splitter (BS_2), a right angle prism (RAP) as the reference mirror, and a retro-reflector (RR) as the moving target. As shown in Fig. 1, two parallel beams, where the solid and dotted line indicating top and bottom beams, respectively, travel to BS_2. The reflected beam travels toward the RAP, which has line symmetry. The transmitted beam travels to the RR, which has point symmetry [17]. When both the reference and measurement beams hit their respective targets, they will change vertical position, i.e. the bottom beam will go to top and vice versa, which allows for the reference and measurement beams to recombine at BS_2 to create interference with opposite phase directions, detected by the photodetectors (PD_R and PD_M). From the PD_R and PD_M, the phase difference $\varphi=8\pi\Delta L/\lambda$ (where ΔL is the displacement of the RR and λ is the wavelength of light), which results in a optical resolution of $\lambda/4$, can be obtained. The main advantage of this interferometer is there is no possibility to generate any leakage beams in the optics, which means periodic nonlinearities are essentially eliminated. Moreover, the optical resolution is doubled without a complicated beam path because the phase direction between two interference signals is opposite. This interferometer was optimized to have minimum optical components as well as no expensive custom optics, so it can be easily applied to industrial and science fields.

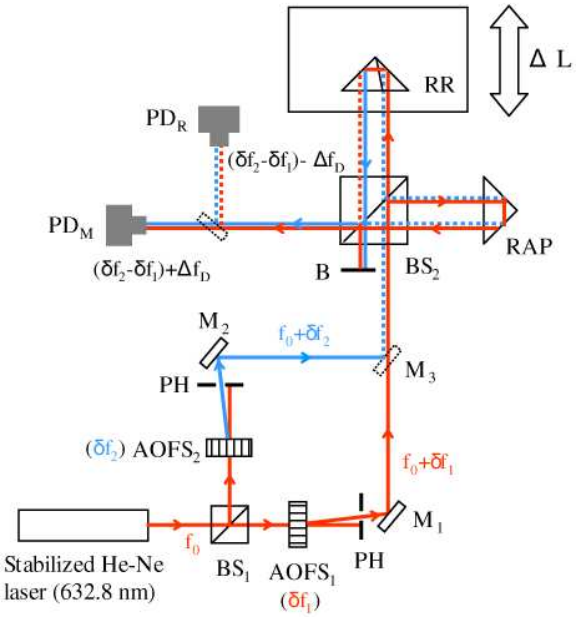

Fig. 1. The optical configuration of a high resolution heterodyne laser interferometer with no detectable periodic nonlinearity; BS_1, BS_2, beams splitters; $AOFS_1$, $AOFS_2$, acousto-optic frequency shifters; PH, pinhole; M_1, M_2, M_3, adjustable mirrors; RR, retro-reflector; RAP, right angle prism; B, beam blocker; PD_R, PD_M, reference and measurement photodetectors, respectively. The dotted line is used to indicate that the beam is at the bottom. Δf_D is the Doppler shift from the stage motion (ΔL).

While the spatially separated source is somewhat complicated, this could be remotely located and the beams could be directed to the interferometer using optical fibers, which is done in most precision industrial applications. This removes a heat source from the interferometer. The frequency stability of the three mode HeNe laser, used as a stabilized source in our research, was on the order of 10^{-10}. The central mode provided approximately 2 mW of power, which is much higher than typical commercial sources. After splitting and

#117076 - $15.00 USD Received 11 Sep 2009; revised 21 Dec 2009; accepted 23 Dec 2009; published 8 Jan 2010
(C) 2010 OSA

frequency shifting, there was approximately 0.75 mW of power per beam (~1.5 mW total), depending on alignment, which can be split for multi-axis systems without significant power loss.

Figure 2 shows the measured wrapped phase of the interferometer compared to a typical heterodyne laser interferometer with a Zeeman split frequency laser (632.8 nm). The phase was measured by a custom built phase meter in a dSPACE data acquisition system, while the retro-reflector in Fig. 1 was translated using a piezoelectric-driven stage (MAX311, Thorlabs). The positioning stage was operated in closed loop and controlled with approximately 20 nm steps. As shown in Fig. 2, the wrapped phase measured in the proposed interferometer is twice as fast as the typical interferometer according to the stage motion. It is noted that the 20 nm step motion was averaged with the low pass filter to simply compare the wrapped phases in Fig. 2. This observation confirms that the optical resolution is improved by a factor of two.

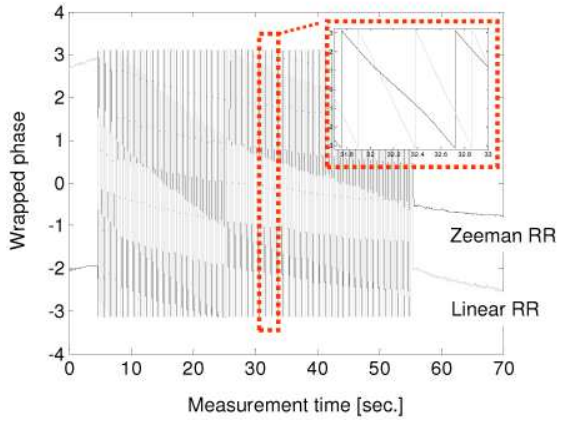

Fig. 2. Measured wrapped phase of the interferometer depicted in Fig. 1 (Linear RR, grey line) and a typical interferometer (Zeeman RR, black line). In both interferometer configurations a retro-reflector is used as a measurement target. The inset means the phase change of our interferometer is twice as faster as that of the typical one.

To evaluate the periodic nonlinearity, the measured displacements were fitted with a low order polynomial to remove the large nonlinear motions of the stage. The residual difference between the measured and fitted data was applied to a fast Fourier transform (FFT) to detect the periodicity [15]. To reduce the noise from undesired stage vibrations, the FFT results of 10 measurements were averaged. Since the nonlinearity shows up as a periodic measurement, the FFT results plotted against the nominal fringe frequency can be used to determine the error based on the fringe order. Figure 3 presents a periodic nonlinearity comparison of the two interferometers according to the fringe order in the FFT domain. It should be noted this method assumes the periodic stage motion errors and mount vibration errors do not occur at the same frequency as the first and second order optical errors.

The periodicity for the typical interferometer using a Zeeman laser was determined to be approximately 7 nm at the first fringe order, as shown in Fig. 3(a). While no periodic nonlinearity is detectable with the proposed interferometer at half, first and second fringe order, several peaks appeared in the Fig. 3(b) however. Those peaks are caused by the residual vibration effects from the stage motion after averaging and resolution limitations of the phase measuring electronics. The peaks appeared apart from the fringe orders while the periodic nonlinearity was below the noise level of approximately 20 pm. The noise level was caused from the electronic measuring board, shot noise of the detectors, and mechanical vibrations, and minimizing these effects is needed to improve the accuracy of this system.

#117076 - $15.00 USD Received 11 Sep 2009; revised 21 Dec 2009; accepted 23 Dec 2009; published 8 Jan 2010
(C) 2010 OSA

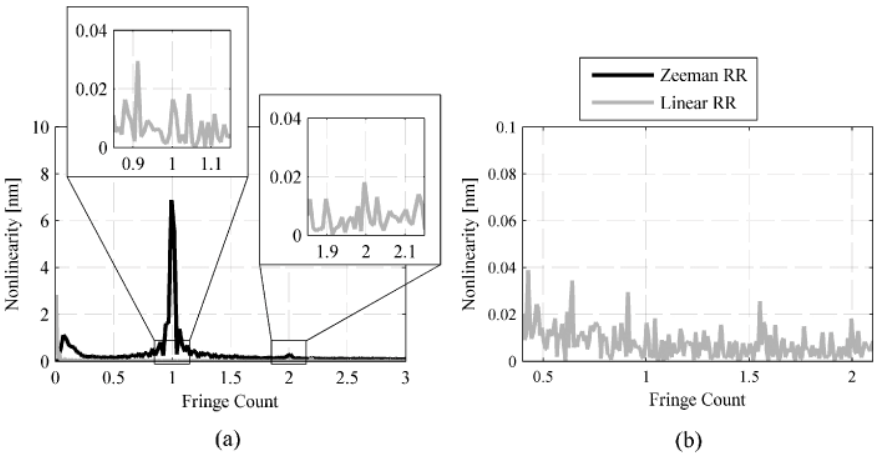

Fig. 3. (a) FFT analysis of the difference between measured displacements and the fitted one in our interferometer (Linear RR, grey line) and the typical interferometer (Zeeman RR, black line), (b) enlargement of the FFT results in the proposed interferometer. The periodic nonlinearity of approximately 7 nm was detected in the typical interferometer while there was no observable periodic nonlinearity in the proposed interferometer except for peaks caused by vibrations.

3. High resolution plane mirror interferometer

The interferometer concept to separate the two beams and use a right angle prism can also be adapted for plane mirror targets, as shown in Fig. 4, which are commonly used in multi-degree of freedom systems. Instead of a retro-reflector target, a plane mirror interferometer (PMI) which consists of a polarizing beam splitter (PBS), a quarter-wave plate (QWP), a retro-reflector (RR) and a flat mirror (M) are included in the basic configuration. In this interferometer, the optical resolution becomes λ/8 (79 nm) because of the double-path interferometer setup. The reference and measurement beams are completely separated until they are recombined by the BS, which eliminates the chances for frequency or polarization mixing. With the exception of ghost reflections, there is also no beam leakage present, thus it is theoretically free from periodic errors. Figure 5 shows the FFT analysis of the experimental displacement results compared to a commercial 2-pass plane mirror interferometer (E1826G, Agilent). Similar to the retro-reflector interferometer case, the wrapped phase was twice faster and no periodic nonlinearity was detected, while the commercial interferometer has the first order nonlinearity of approximately 0.3 nm, as shown in Fig. 5(a). Although several peaks appeared in the FFT domain, these peaks originate from the stage motion vibrations. Because of the optical resolution doubling, these vibration peaks shift to half the original frequency between the Agilent PMI measurements and our Linear PMI measurements. The three peak pairs are shown in Fig. 5(b), where the fringe order is halved between the two measurements but the amplitude is approximately the same.

#117076 - $15.00 USD Received 11 Sep 2009; revised 21 Dec 2009; accepted 23 Dec 2009; published 8 Jan 2010
(C) 2010 OSA

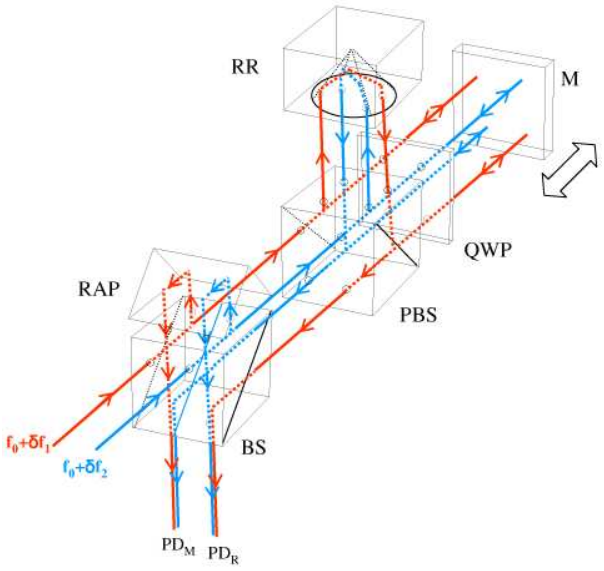

Fig. 4. The schematic of plane mirror interferometer with two spatially separated beams and right angle prism; BS, beams splitter; PBS, polarizing beam splitter; QWP, quarter-wave plate; RR, retro-reflector; RAP, right angle prism; M, target mirror; PD_R, PD_M, reference and measurement photodetectors, respectively.

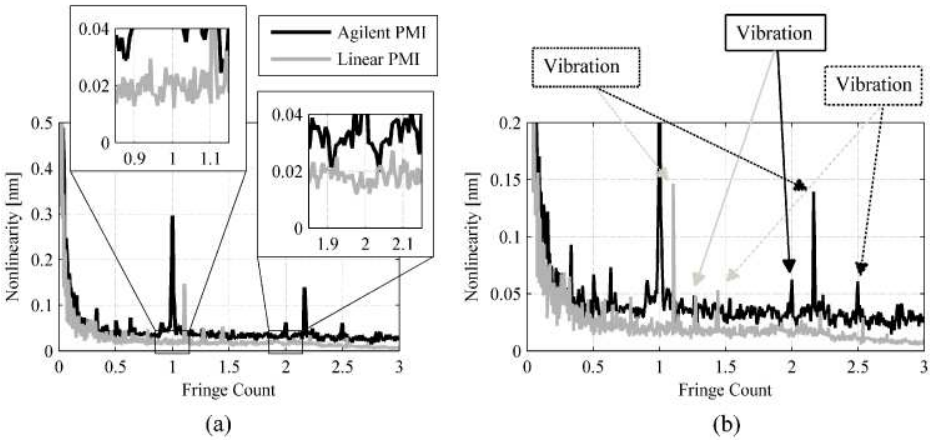

Fig. 5. (a) FFT analysis of the difference between measured displacements and the fitted one in the proposed interferometer (Linear PMI, grey line) and the commercial interferometer (Agilent PMI, black line), (b) indicating several peaks caused by stage vibrations in both of the results. The peaks of the commercial interferometer were matched with the peaks of our interferometer considering the optical resolution.

4. Discussion

The drawback of the linear plane mirror interferometer in Section 3 is that the configuration is unbalanced between the reference and measurement paths. Due to the additional path of the measurement beam in the optical components such as a PBS and a QWP, temperature fluctuations can give rise to the significant thermal errors in the interferometer. To avoid or minimize these thermal errors, a differential type plane mirror interferometer was considered

#117076 - $15.00 USD Received 11 Sep 2009; revised 21 Dec 2009; accepted 23 Dec 2009; published 8 Jan 2010
(C) 2010 OSA

in this research. Figure 6 shows the proposed plane mirror interferometer which has the differential path between the reference and measurement mirrors. Although this interferometer is not perfectly balanced, the configuration is nearly balanced, so the thermal effects on the optical components can be reduced.

The two parallel beams are divided by a linear displacement beam splitter (DBS) into two sets, reference beams and measurement beams. Similar to a typical plane mirror interferometer, each set of beams has the double-path between a PBS and mirrors. The measurement beams are reflected by a RR experiencing the point symmetry while the reference beams have the line symmetry with a RAP. The two sets of beams propagate back to the DBS and are then recombined to make the heterodyne signals. The heterodyne signals from photodetectors, PD_R and PD_M, again have phase changes in the opposite directions induced by the Doppler shift and are used for reference signal and measurement signal respectively. In this interferometer, the optical resolution is also λ/8 because of the double-path interferometer setup.

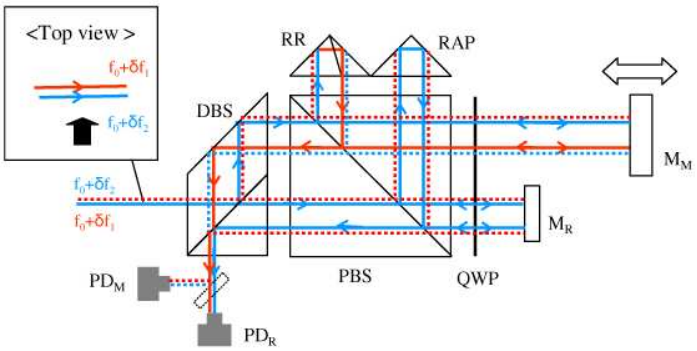

Fig. 6. The differential plane mirror interferometer configuration; DBS, displacement beams splitter; PBS, polarizing beam splitter; QWP, quarter-wave plate; RR, retro-reflector; RAP, right angle prism; M_R, M_M, reference and measurement mirrors; PD_R, PD_M, reference and measurement photodetectors, respectively. The dotted line is used to indicate that the beam is at the bottom.

5. Conclusion

In this paper, a heterodyne laser interferometer with no detectable periodic nonlinearity was proposed and verified. This interferometer used two spatially separated beams to prevent any source mixing and polarization leakage. Moreover, the optical resolution was enhanced by a factor of two due to the opposite phase change direction between reference and measurement signals. To verify our interferometer, a retro-reflector and plane mirror interferometer configurations were tested and compared with typical interferometers. The optical resolution enhancement was confirmed and the periodic nonlinearity was below the measurement noise level, which was approximately 20 pm.

This work was supported by the Dutch IOP (projects IPT06104 and IPT04001) in the Netherlands. The authors would like to acknowledge Agilent Technologies and VSL Dutch Metrology Institute for their equipment support.

#117076 - $15.00 USD Received 11 Sep 2009; revised 21 Dec 2009; accepted 23 Dec 2009; published 8 Jan 2010
(C) 2010 OSA

Appendix B.3

Article:
Fiber coupled sub nanometer displacement interferometry without periodic nonlinearity

This third article shows the research presented at the 10th International Symposium of Measurement Technology and Intelligent Instruments (ISMTII) from June 29 till July 2nd, 2011 in South Korea (included in *Appendix B.3*). The results described in *Article I: Fiber-coupled displacement interferometry without periodic nonlinearity*, originate from this research.

Fiber coupled sub nanometer displacement interferometry without periodic nonlinearity

Arjan J.H. Meskers[1], Jonathan D. Ellis[1,2], Jo W. Spronck[1,*], and Robert H. Munnig-Schmidt[1]

1 PME: Mechatronic System Design, Delft University of Technology, Mekelweg 2, 2628 CD Delft, The Netherlands
2 Now at: Mechanical Engineering Department & Institute of Optics, University of Rochester, Hopeman Building, Rochester, NY, 14627, USA
* Corresponding Author / E-mail: j.w.spronck@tudelft.nl, TEL: +31-15-278-1824, FAX: +31-15-278-2150

KEYWORDS : Displacement Interferometry, Fiber Coupling, Periodic Nonlinearity, Stage Metrology

Displacement interferometers are widely used in precision engineering and metrology applications. For multi-axis systems, free space delivery of the optical beams requires high tolerance pointing stability and couples the source to the interferometer location. Fiber delivery is desired to decouple the source and interferometer but configurations which have to be used for this, contribute typical errors such as periodic nonlinearity. In this paper, we describe a fiber-coupled Joo-type interferometer. Spatial separation of the input beams in this type of interferometer eliminate periodic nonlinearities. This is contrasted by typical heterodyne interferometer systems which have two orthogonal, coaxial beams with a difference frequency. We present the interferometer design, discuss the fiber deployment, and compare free-space and fiber-coupled versions. The results indicate that fiber-induced disturbances are rejected as theory predicts and no periodic nonlinearity was detected.

Manuscript received: January XX, 2011 / Accepted: January XX, 2011

1. Introduction and Motivation

Heterodyne displacement measuring interferometry has been widely used to calibrate other measurement tools such as capacitive sensors, inductive sensors, and optical encoders because of its high dynamic range, high signal-to-noise ratio, and direct traceability to the length standards [1]. Sub-nanometer level measurements must be achieved to satisfy industrial demands on performance [2]. The main error sources that limit the performance are the laser frequency stability [1], refractive index fluctuations in non-common optical paths [3], and periodic nonlinearity [4-6] in the measured phase due to source mixing, manufacturing tolerances, and imperfect alignment.

While the effects of the laser frequency stability and refractive index fluctuations can be mitigated by employing a highly stable reference laser and by performing the measurements in a well controlled environment, the periodic nonlinearity is difficult to eliminate. Moreover, for practical, modular interferometry systems, fiber delivery is desired to decouple the laser source (essentially a large heat source) from the interferometer. Decoupling the laser and interferometer also removes pointing stability effects between the two.

In this paper, we present a comparison between a free-space delivered and a polarization maintaining-fiber (PM-fiber) delivered generalized Joo-type interferometer, developed at the TU Delft. This interferometer type builds on previous research, as presented at the ISMTII in 2009 [7], which demonstrated no detectable periodic nonlinearity (down to the noise floor) in a practical interferometer configuration [8, 9]. The generalized Joo-type interferometer uses two spatially separated source beams with a known frequency difference, rather than the traditional coaxial, orthogonally polarized source beam. By eliminating all beam overlaps until the final interference element, periodic nonlinearity is significantly reduced [10-13]. However, when fiber delivery is applied, the extinction ratio of the fibers and stress induced birefringence can cause frequency mixing which will re-introduce the originally avoided periodic nonlinearity. Additionally, small fiber length changes will appear as Doppler shifts in the main interference signal and can be misinterpreted as stage motions. This interferometer configuration has several advantageous features which can be leveraged to reduce these effects. Simple polarization cleanup on the input beams can limit the fixing due to the fibers. Also, an optical reference is generated within the interferometer block, which will eliminate fiber-induced Doppler shifts and can reduce periodic nonlinearity [14, 15].

2. Modular Fiber Coupled System Concept

System modularity plays an important role for practical purposes in industry. Creating a modular 'plug-and-play' system will decrease system set up time and errors. Current free space systems lack this

robustness and are time consuming during installation due to high demands on pointing stability and alignment over long optical paths. The modular system proposed in this paper, as shown in Figure 1, utilizes fiber coupled delivery of source light towards the interferometer and fiber coupled delivery of the measurement signals to the phasemeter. Additionally, for these experiments, the initial heterodyne optical reference signal is generated at the source to assess fiber-induced Doppler shifts. This concept reduces the pointing stability requirements to just the tolerances in the optic block itself, rather than all components between it and the source. Also, fibers provide simple, flexible beam routing rather than fixed mirrors and splitters which require stable mounting and potentially unstable alignment mechanisms.

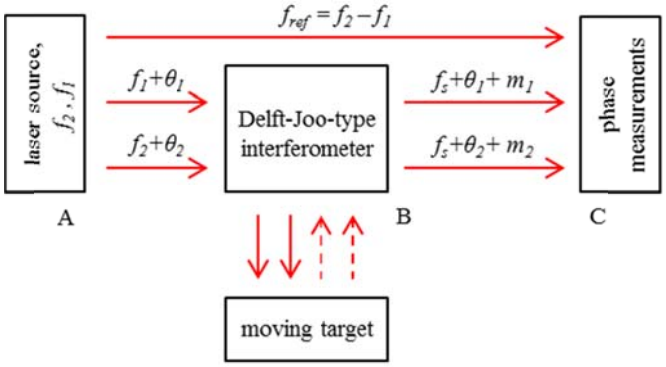

Figure 1: Schematic of the modular interferometry system using fiber couplings to eliminate high alignment accuracy, in between source (A), interferometer (B), and phasemeter (C).

The measurement system proposed can be divided up into three different modules to form the complete system. Module A contains the stabilized laser, components to generate two spatially separated input beams, f_1 and f_2 and the optical reference signal before the fibers, f_{ref}. The beams for the interferometer are then launched into PM-fibers while the optical reference is launched into multimode-fibers (MM fibers). The fiber-fed input beams are then sent to the interferometer, which is described in more detail in the next section. The interference signals, both from the interferometer and optical reference, are sent via MM-fibers to a phasemeter. The optical reference frequency is directly connected to the phasemeter (N1225A, Agilent) for phase measurement and post processing to determine the fiber-induced effects.

Figures 2 and 3 show the heterodyne frequency generation schematic and a photograph of our implementation, respectively. A frequency stabilized 633 nm HeNe laser is isolated from feedback using a free space optical isolator, OI. The beam is then split equally (BS_1) and each beam is frequency upshifted by an AOM, one at 39 MHz and the other at 41 MHz.

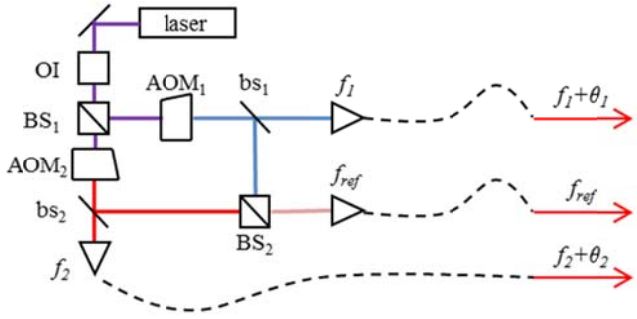

Figure 2: Schematic of the source and heterodyne frequency generation. A stabilized laser is optically isolated and split equally before passing through two AOMs driven at 39 MHz and 41 MHz, respectively. Both first order upshifted beams are transported to the interferometer, while also an optical reference signal is generated.

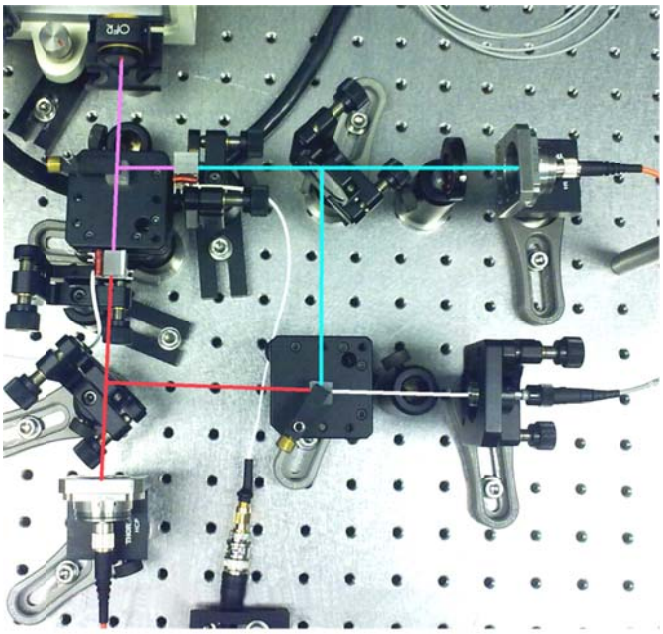

Figure 3: Photograph of our heterodyne frequency generation scheme.

An optical reference is generated at 2 MHz by using two beam samplers ($bs_{1,2}$) and a beamsplitter (BS_2) to interfere the upshifted beams. The main parts of each upshifted beam is either steered into the interferometer (in the free-space system) or launched into two PM fibers (for the fiber coupled system).

3. Generalized Joo-interferometer Design

Periodic nonlinearities are typically eliminated in heterodyne interferometry systems by only allowing the reference and measurement arms to overlap at the main interfering element [refs]. In all other instances, the beams remain separate. Figure 4 shows a schematic of the Generalized Joo-type interferometer used in this research. The two spatially separated input beams ($f_1+\theta_1$, $f_2+\theta_2$) with a slightly different optical frequency are sent to the interferometer. Two reference arms are generated by splitting 50% from a beam splitter (BS) and passing them to a large retroreflector (RR). The two beams reflect diagonally from the (large) RR and are shifted to a lower plane upon exiting, going into PD_m and PD_r and serve as reference beams. They then pass back to the BS where they interfere with their respective measurement arms.

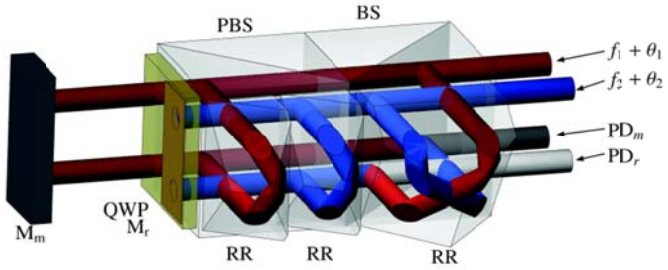

Figure 4: Schematic of the Generalized Joo-type interferometer. Two spatially separated input beams are sent to the interferometer which has a measurement interferometer and a reference interferometer to remove fiber-induced Doppler shifts. (In our implementation, a single right angle prism was used instead of two small retroreflectors for simplicity.)

The measurement arms are generated from the beams that initially transmit through the BS and transmit through a polarizing beam-splitter (PBS) and quarter wave plate (QWP) on the way to their respective mirrors. One is a fixed mirror to generate the reference

signal (M_r) and the other is a mirror mounted to the moving stage (M_m). Upon reflecting, both beams pass through the QWP for a second time where they reflect in the PBS. The beams reflect from two smaller RRs and are displaced to the same lower plane as their reference beams were displaced in the big RR. They then reflect in the PBS again and transmit through the QWP, where they hit their respective targets for a second time. They then transmit through the QWP, PBS and interfere with their reference arms in the BS. In our specific implementation, we replaced the two smaller RRs with a right angle prism (RAP), which performs essentially the same function.

Two signals, I_m and I_r are detected from fiber-coupled photo-detectors PD_m and PD_r, respectively. The two interference signals take the form of

$$I_m \propto \cos\left(2\pi f_1 t + \theta_1\right) \cdot \cos\left(2\pi f_2 t + \theta_2 + \theta_m\right) \quad (1)$$

$$I_r \propto \cos\left(2\pi f_2 t + \theta_2\right) \cdot \cos\left(2\pi f_1 t + \theta_1 + \theta_r\right) \quad (2)$$

where f_1 and f_2 are the two optical frequencies from the source, θ_1 and θ_2 are the phases of the two input beams (continuously changing due to the air-path/fibers, with $\theta_1 \neq \theta_2$), and θ_m and θ_r are the measured Doppler shifts due to mirror displacements. According to the trigonometric identity

$$2\cos A \cos B = \cos\left(A + B\right) + \cos\left(A - B\right) \quad (3)$$

Equations (1) and (2) can be rewritten with the additive components ignored because their frequencies are too high to detect. The resulting interference signals are

$$I_m \propto \cos\left(2\pi\left(f_1 - f_2\right)t + \theta_1 - \theta_2 - \theta_m\right) \quad (4)$$

$$I_r \propto \cos\left(2\pi\left(f_2 - f_1\right)t - \theta_1 + \theta_2 - \theta_r\right) \quad (5)$$

Assuming $f_1 - f_2 = f_s$, which is the 2 MHz split frequency, Equations (4) and (5) can be rewritten as

$$I_m \propto \cos\left(2\pi f_s t + \theta_1 - \theta_2 - \theta_m\right) \quad (6)$$

$$I_r \propto \cos\left(2\pi f_s t + \theta_1 - \theta_2 + \theta_r\right) \quad (7)$$

Using a similar procedure, it can be shown the irradiance of the optical reference signal, I_{or} , which is generated prior to the beam transport, is

$$I_{or} \propto \cos\left(2\pi f_s t\right) \quad (8)$$

If the optical reference is used for the phase measurement, then the difference between the phase fluctuations in the fibers appears as a Doppler shift in the measurement. However, the phase difference between I_m and I_r includes the fiber-induced phase changes, which cancels when the difference is measured ($(\theta_1-\theta_2+\theta_r)-(\theta_1-\theta_2-\theta_m) = (\theta_r+\theta_m)$). When the reference mirror is stationary ($\Delta\theta_r$ is zero), which is assumed for most displacement interferometers, the measured phase change equals the phase change of the measurement path ($\Delta\theta_m$). Assuming the refractive index and wavelength are constant, the measured phase change is then

$$\Delta\theta_m = \frac{2\pi N n \Delta x}{\lambda_2} \quad (9)$$

where N is the interferometer fold constant (four in this interferometer), n is the refractive index, λ_2 is the wavelength, and Δx is the displacement of the measurement mirror.

4. Free Space Generalized Joo-Interferometer System

The Generalized Joo-type interferometer was constructed using free space beam delivery and fiber-coupled detection, which can be seen in Figures 5 and 6. The measurement mirror was mounted to a linear air bearing stage (ABL1000, Aerotech), which has a 100 mm displacement range. Each measurement consists of a forward stage displacement, followed by a pause, and then a backwards stage displacement, all performed at constant velocity. During the stage displacement the mirror moved with a constant velocity, measurements were performed at 10 nm/s, 100nm/s, 1 μm /s, 10 μm /s and 100 μm/s.

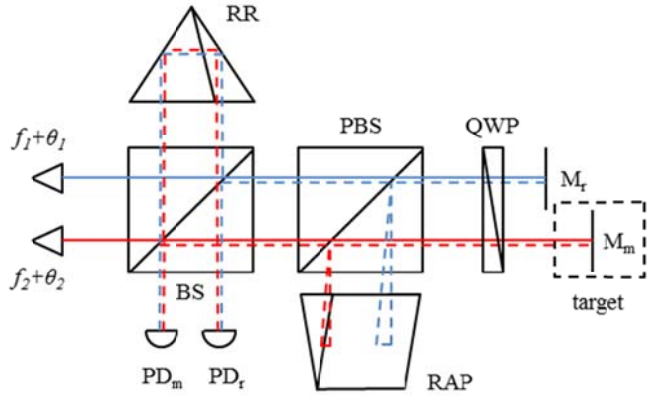

Figure 5: Schematic of the Generalized Joo-type interferometer. The spatially separated source beams come in including the phases θ_1 and θ_2 originating from either air-path or fiber induced disturbances. Detection takes place with PD_m and PD_r which are MM-fiber coupled to the phase meter (Agilent N1225A).

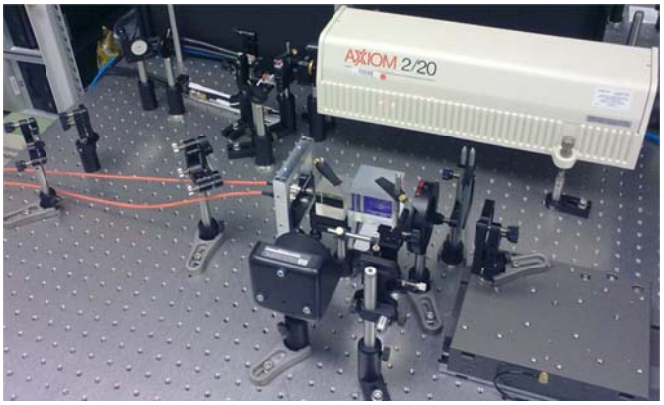

Figure 6: Photograph of the free space delivery system, interferometer and stage measurement setup. The two interference beams from the interferometer are detected and measured using MM-fiber and fiber-coupled detectors. The generation of the reference signal as depicted in Fig. 2 is not used in this setup.

The sampling rate and stage displacements are coupled in our case because only a limited number of points can be sampled using our interface with the phasemeter. At each velocity we sampled the maximum number of points (around 700k data points) and ensured that the sample rate was sufficient to measure and assess second order periodic nonlinearity in the measurements.

Figure 7 shows the displacement measured with the stage moving at a constant velocity of 10 nm/s. "Joo Gen" is the measured length change from the phase difference between I_r and I_m from PD_r and PD_m respectively. The Joo Gen signal closely follows the stage drive signal ("Path"), with minor fluctuations due to acoustic interference and refractive index changes. The relative error of these fluctuations decreases as the stage moves at higher velocity, as shown in Figure 8.

The linear forwards and backwards section were analyzed for each of the different velocities. Figure 9 shows the amplitude spectrum for the 100 μm/s velocity measurement as a function of Fringe Order which is typically used to analyze periodic errors.

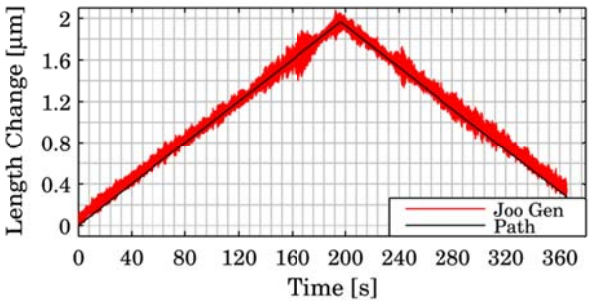

Figure 7: Stage measurement at 10 nm/s forwards and backwards. The air-path-induced Doppler shifts cause errors at nanometer level which clearly shows up at low velocities.

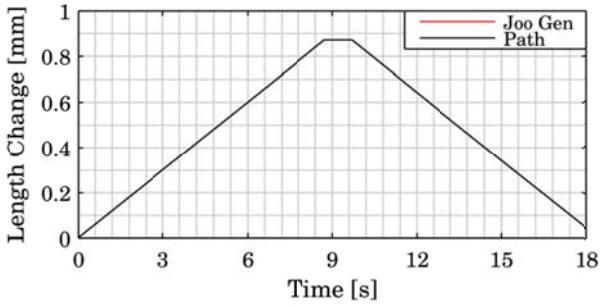

Figure 8: At 100 μm/s forwards and backwards, the air-path fluctuations are much smaller relative to the overall motion. The measured path and commanded path both nominally overlap.

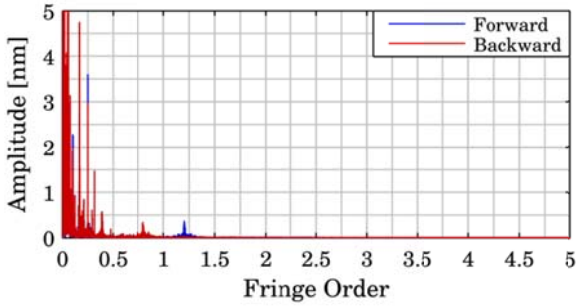

Figure 9: Periodic error analysis of the free-space 100 μm/s measurement. The amplitude spectrum after removing a first order polynomial and converting to the frequency domain for fringe spacing revealed no detectable periodic errors.

In this measurement, there are clearly no first or second order periodic errors present and the peaks at the lower fringe orders are due to noise in the surrounding environment. This measurement is indicative of the other measurements taken spanning from 10 nm/s to 1 mm/s. In all measurements, the only peaks that occurred at the first and second fringe orders occurred due to vibrations coincidentally overlapping because the fringe passing frequency and vibration frequencies were matched.

The noise in the surrounding environment that was observed in all measurements lays around 34 Hz, see Figure 14. This noise is attributed to laboratory acoustic interference, vibrations, and refractive index fluctuations, which also have been observed in other measurements in the laboratory.

5. Fiber Coupled Generalized Joo-Interferometer System

The Generalized Joo-type interferometer as shown in Figure 5 was tested at the same velocities as its free-space counterpart. Figure 10 shows a photograph of the fiber-coupled setup. The phase differences between I_r, I_m, and I_{ref} were all measured to assess both the fiber fluctuations and the stability of the reference arm in the interferometer.

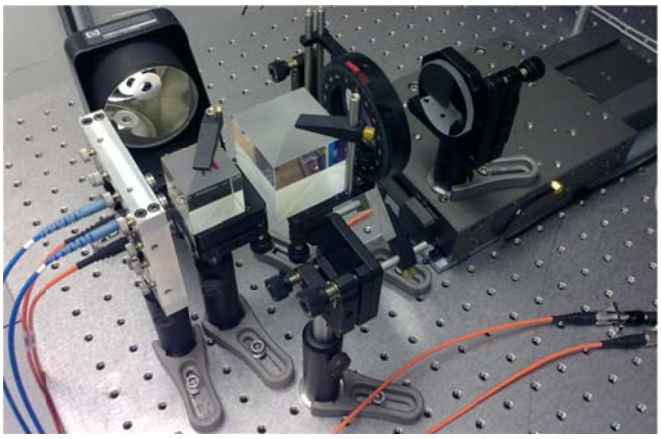

Figure 10: Photograph of our measurement setup with PM fiber coupled source beam delivery. The setup and detection are identical to the scheme in Fig. 4 and the setup in Fig. 5 except for the fiber delivery.

Figure 11 shows the measured displacement with the stage moving at a constant velocity of 10 nm/s. Displacement "Ref" is the measured length change from the phase difference between difference between I_{ref} and I_r. "Meas" is the difference between I_{ref} and I_m. Both of these signals show considerable drift which is can be attributed to fiber-induced Doppler shifts. "Joo Gen" is the measured length change from the phase difference between I_r and I_m, which cancels the fiber-induced Doppler shifts. The Joo Gen signal follows the stage drive signal ("Path"), with small fluctuations due to acoustic interference and refractive index fluctuations. When the fiber effects are not canceled and the stage motion is slow, the fibers can induce large errors. When the stage velocity is higher, as shown in Figure 12 where the velocity is 100 μm/s, the fiber fluctuations are smaller, but still cause errors on the micrometer level if it is not taken into account.

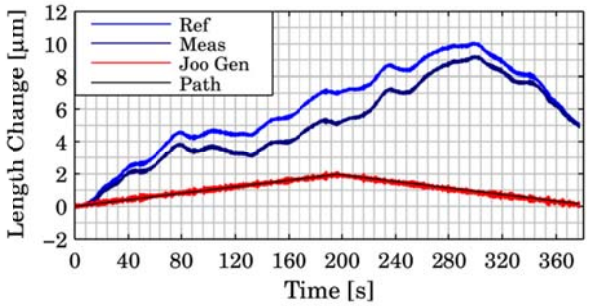

Figure 11: Stage measurement at 10 nm/s forwards and backwards. The fiber-induced Doppler shifts cause errors at the micrometer level which can be clearly seen at low velocities.

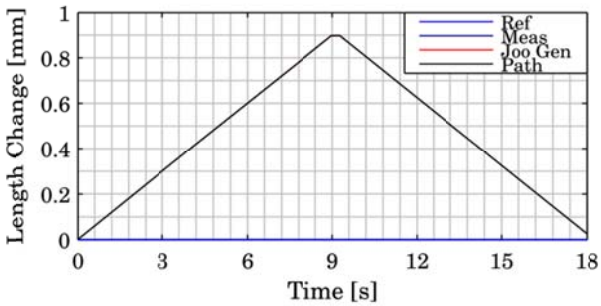

Figure 12: At 100 μm/s forwards and backwards, the fiber fluctuations appear much smaller relative to the overall motion but still contribute errors on the order of micrometers. Meas, Joo Gen, and Path all nominally overlap in this instance.

Also for this interferometer configuration, the linear forwards and backwards section were analyzed for each of the different velocities. Figure 15 shows the amplitude spectrum as a function of Fringe Order for the 100 µm/s velocity measurement which clearly shows no observable periodic errors.

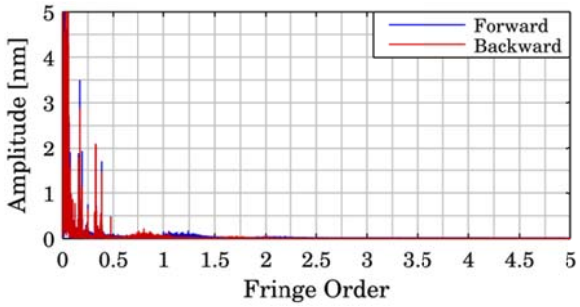

Figure 13: Periodic error analysis of the fiber-coupled 100 µm/s measurement. Correlation with the frequency domain for fringe spacing revealed no detectable periodic errors.

When the frequency spectrum is converted to Fringe Order based on the nominal fringe spacing, also for this measurement setup, the peaks shift with an order of magnitude spacing between them, as shown in Figure 15. From the results from the fiber coupled measurements peaks can be observed at the first and second order harmonics, which shift when different sampling and velocity parameters are changed. This means the peaks also here are not attributed to periodic nonlinearity. Thus, we conclude that this interferometer configuration in both its free-space and fiber-delivered configuration has no detectable periodic nonlinearity.

Figure 16 shows a comparison between free-space and fiber coupled measurements at 100 µm/s. The free-space measurement shows sharper peaks in the amplitude spectrum than the fiber-coupled version. Because the fibers create a continuous frequency shift at the micrometer level, some peaks are attenuated which can be advantageous for high frequency feedback stages. The lower order vibrations are likely due to the surrounding environment while the symmetric peaks around the first order are due to stage motions. The forwards and backwards motions of the stage cause opposite Doppler shifts, which will be reflected in the measurement if the stage motion or mirror mount on the stage are vibrating due to the motion.

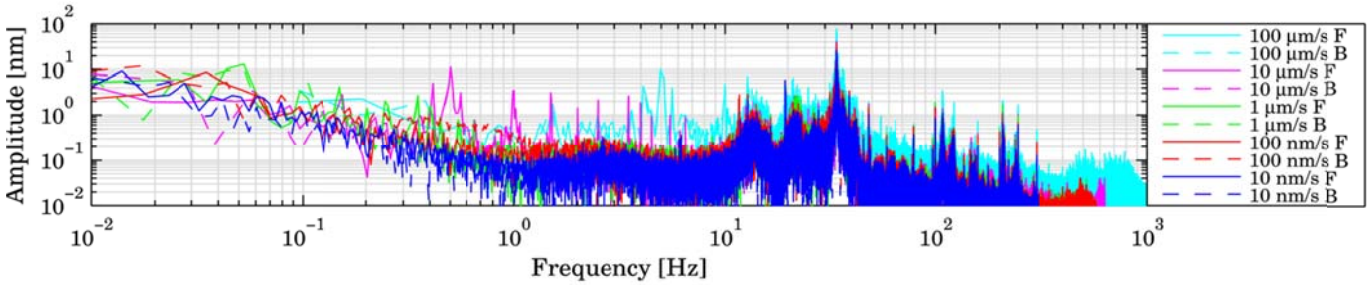

Figure 14: Amplitude spectrum based on the sampling frequency for various stage motion velocities. There is a common noise level in the range of 10 Hz to 40 Hz and at higher peaks which can be seen in all measurements. The higher noise levels in the faster measurements (100 µm/s and 10 µm/s) is likely due to increased vibrations from the stage motion and instability in the mirror mount.

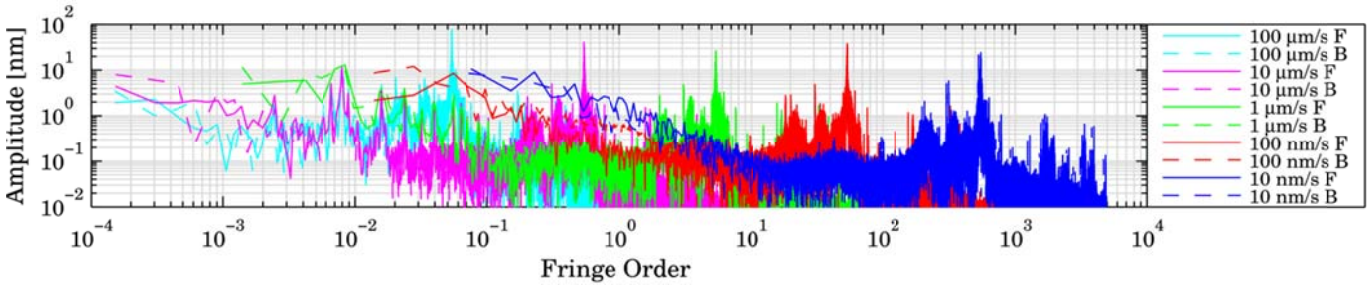

Figure 15: Amplitude spectrum based on the fringe passing frequency to determine the error amplitude based on Fringe Order. Typically periodic nonlinearity occurs at the first and second fringe orders. Because these peaks shift as a function of velocity but not sampling frequency, they can be attributed to vibrations rather than periodic error. This is particularly for the 1 µm/s measurements which has a clear peak at the first fringe order but has matched peaks shifted by an order of magnitude as the velocity changes by equal order of magnitude.

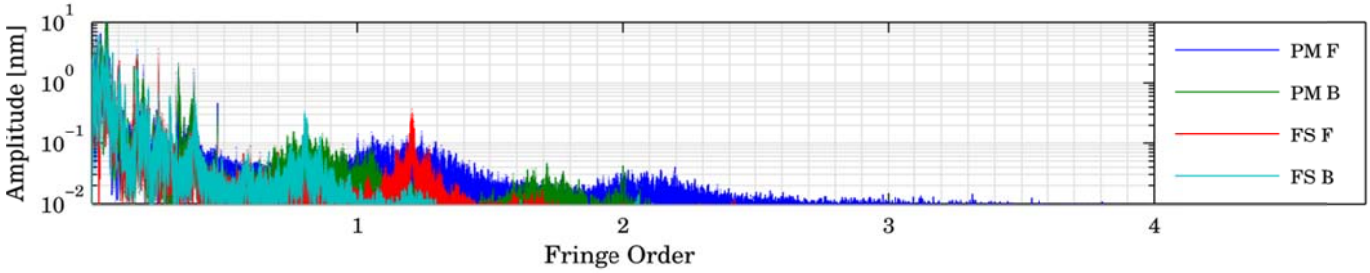

Figure 16: Amplitude spectrum of Figures 9 and 13 combined. The peaks for the free-space setup are much sharper than the broad 'peaks' from the fiber coupled setup. The forward and backward travel of the stage shows symmetry around a fringe order of 1 which is related to the positive and negative Doppler shift depending on the direction of stage travel.

6. Conclusions

Two types of beam delivery were designed, built, and tested for the Generalized Joo-type interferometer, one with free-space delivery and one with PM optical fiber delivery. The free-space and fiber-delivered systems used essentially the same components, with the exception of the fiber couplers themselves and beam steering mirrors for the free space setup. The fiber coupled system has an advantage of being completely decoupled from the source, while still contributing no periodic nonlinearity and self correcting for false fiber-induced displacements.

Measurements with the fiber coupled configuration have showed that the system is capable of operating at the same or at a lower noise level than the free-space beam delivery setup. Linear displacements and frequency domain analysis techniques were employed to assess the periodic nonlinearity and deconvolve it from spurious vibrations and refractive index fluctuations.

This research shows a highly modularized displacement interferometry system without free-space beam delivery paths, which can be suitable for sub-nanometer measurements.

ACKNOWLEDGEMENTS

This work was performed at the Delft University of Technology and supported by the Dutch IOP (IPT04001) in the Netherlands. The authors are grateful for the support by Agilent Technologies for providing the phase measurement board used during these measurements. The authors would like to thank the IOP User Committee for many fruitful discussions regarding this research.

REFERENCES

1. Bobroff, N., “Recent advances in displacement measuring interferometry”, Measurement Science and Technology, Vol. 4, No. 9, pp. 907-926, 1993.
2. Demarest, F.C., “High-resolution, high-speed, low data age uncertainty, heterodyne displacement measuring interferometer electronics”, Measurement Science and Technology, Vol. 9, No. 7, pp. 1024-1030, 1998.
3. Tyler Estler, W., “High-accuracy displacement interferometry in air”, Applied Optics, Vol. 24, No. 6, pp. 808-815, 1985.
4. Quenelle, R.C., “Nonlinearity in interferometer measurements”, Hewlett Packard Journal, Vol. 34, pp 10, 1983.
5. Hou, Wenmei, Wilkening and Gunter, “Investigation and compensation of the nonlinearity of heterodyne interferometers”, Precision Engineering, Vol. 14, No. 2, pp 91-98, 1992.
6. De Freitas, J. M. and Player, M. A., “Polarization Effects in Heterodyne Interferometry”, Journal of Modern Optics,Vol. 42, No. 9, pp. 1875-1899, 1995.
7. Joo, K.N., Ellis, J.D., Spronck, J.W., van Kan, P.J.M. and Munnig Schmidt, R.H., “Simple heterodyne laser interferometer without periodic errors”, Proc. 9th ISMTII, 29 Jun-2July, St. Petersburg, Russia, 2009.
8. Joo, K.N., Ellis, J.D., Spronck, J.W., van Kan, P.J.M. and Munnig Schmidt, R.H., “Simple heterodyne laser interferometer with subnanometer periodic errors”, Optics Letters, Vol. 34, No. 3, pp. 386-388, 2009.
9. Joo, K.N., Ellis, J.D., Spronck, J.W., Buice, E.S., Spronck, J.W. and Munnig Schmidt, R.H., “High resolution heterodyne interferometer without detectable periodic nonlinearity”, Optics Express, Vol. 18, No. 2, pp. 1159-1165, 2010.
10. Tanaka, M., Yamagami, T. and Nakayama, K., “Linear interpolation of periodic error in a heterodyne laser interferometer at subnanometer levels [dimension measurement]”, IEEE Transactions on Instrumentation and Measurement, Vol. 38, No. 2, pp. 552-554, 1989.
11. Wu, C., Lawall, J., and Deslattes, R.D., “Heterodyne Interferometer with Subatomic Periodic Nonlinearity”, Applied Optics, Vol. 38, No. 19, pp. 4089-4094, 1999.
12. Lawall, J., and Kessler, E., “Michelson interferometry with 10 pm accuracy”, Review of Scientific Instruments, Vol. 71, No. 7, pp. 2669-2676, 2000
13. Schuldt, H., Gohlke, M., Weise, D., Johann, U., Peters, A. and Braxmaier, C., “Picometer and nanoradian optical heterodyne interferometry for translation and tilt metrology of the {LISA} gravitational reference sensor”, Classical and Quantum Gravity, Vol. 26, No. 8, pp. 085008, 2009.
14. Knarren, B.A.W.H., “Application of optical fibres in precision heterodyne laser interferometry”, PhD Thesis, Technical University of Eindhoven, Netherlands, 2003.
15. Knarren, B.A.W.H., Cosijns, S.J.A.G., Haitjema, H., and Schellekens, P.H.J., “Validation of a single fibre-fed heterodyne laser interferometer with nanometre uncertainty”, Precision Engineering, Vol. 2, pp. 229-236, 2005